International Journal of Biological Macromolecules 277 (2024) 134079

Contents lists available at ScienceDirect

International Journal of Biological Macromolecules

journal homepage: www.elsevier.com/locate/ijbiomac

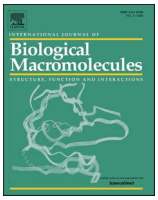

Effectiveness of gellan gum scaffolds loaded with *Boswellia serrata* extract for *in-situ* modulation of pro-inflammatory pathways affecting cartilage healing

Stefania Cometa [a], Francesco Busto [b,c], Alessandro C. Scalia [d], Andrea Castellaneta [b], Piergiorgio Gentile [e], Andrea Cochis [d], Marcello Manfredi [f], Vittoria Borrini [f], Lia Rimondini [d], Elvira De Giglio [b,c,*]

[a] *Jaber Innovation s.r.l., Via Calcutta 8, 00144 Rome, Italy*
[b] *Department of Chemistry, University of Bari, Via Orabona 4, 70126 Bari, Italy*
[c] *INSTM, National Consortium of Materials Science and Technology, Via G. Giusti 9, 50121 Florence, Italy*
[d] *Center for Translational Research on Autoimmune and Allergic Disease, CAAD, Department of Health Sciences, Università del Piemonte Orientale, 28100 Novara, Italy*
[e] *Newcastle University, School of Engineering, Claremont Road, NE1 7RU Newcastle upon Tyne, United Kingdom*
[f] *Center for Translational Research on Autoimmune and Allergic Disease, CAAD, Department of Translational Medicine, Università del Piemonte Orientale, 28100 Novara, Italy*

ARTICLE INFO

Keywords:
Gellan gum
Boswellia serrata extract
Anti-inflammatory
Chondrogenesis
Mechanical reinforcement

ABSTRACT

In this study, we developed a composite hydrogel based on Gellan gum containing *Boswellia serrata* extract (BSE). BSE was either incorporated directly or loaded into an MgAl-layered double hydroxide (LDH) clay to create a multifunctional cartilage substitute. This composite was designed to provide anti-inflammatory properties while enhancing chondrogenesis. Additionally, LDH was exploited to facilitate the loading of hydrophobic BSE components and to improve the hydrogel's mechanical properties. A calcination process was also adopted on LDH to increase BSE loading. Physicochemical and mechanical characterizations were performed by spectroscopic (XPS and FTIR), thermogravimetric, rheological, compression test, weight loss and morphological (SEM) investigations. RPLC-ESI-FTMS was employed to investigate the boswellic acids release in simulated synovial fluid. The composites were cytocompatible and capable of supporting the mesenchymal stem cells (hMSC) growth in a 3D-conformation. Loading BSE resulted in the modulation of the pro-inflammatory cascade by down-regulating COX2, PGE2 and IL1β. Chondrogenesis studies demonstrated an enhanced differentiation, leading to the up-regulation of COL 2 and ACAN. This effect was attributed to the efficacy of BSE in reducing the inflammation through PGE2 down-regulation and IL10 up-regulation. Proteomics studies confirmed gene expression findings by revealing an anti-inflammatory protein signature during chondrogenesis of the cells cultivated onto loaded specimens. Concluding, BSE-loaded composites hold promise as a tool for the *in-situ* modulation of the inflammatory cascade while preserving cartilage healing.

1. Introduction

Cartilage repair remains a significant challenge for the orthopaedic community, and osteoarthritis has become a global health priority due to the increasing aging population. Unfortunately, current strategies often fail short of achieving full tissue regeneration because damaged cartilage is inherently difficult to self-recover due to its avascular, aneural, and nonlymphatic properties [1].

Among the recognized factors contributing to cartilage repair issues, inflammation plays a major role in healing failure. When pro-inflammatory conditions persist for extended periods, they can lead to chronic diseases, resulting in general cartilage degeneration due to the loss of proper biomechanical properties (creep and stress relaxation) and unwanted infiltration of blood vessels [2]. One common clinical

* Corresponding author at: Department of Chemistry, University of Bari "Aldo Moro", via E. Orabona 4, 70126 Bari, Italy.
E-mail addresses: stefania.cometa@jaber.it (S. Cometa), f.busto3@studenti.uniba.it (F. Busto), alessandro.scalia@uniupo.it (A.C. Scalia), andrea.castellaneta@uniba.it (A. Castellaneta), piergiorgio.gentile@newcastle.ac.uk (P. Gentile), andrea.cochis@med.uniupo.it (A. Cochis), marcello.manfredi@uniupo.it (M. Manfredi), vittoriafederica.borrini@uniupo.it (V. Borrini), lia.rimondini@med.uniupo.it (L. Rimondini), elvira.degiglio@uniba.it (E. De Giglio).

https://doi.org/10.1016/j.ijbiomac.2024.134079
Received 6 November 2023; Received in revised form 9 May 2024; Accepted 19 July 2024
Available online 20 July 2024

approach to managing these pro-inflammatory conditions involved the intra-articular injection of glucocorticoids (GCs). These GCs offer local relief, reducing pain, increasing mobility, and generally improving patients' quality of life [3]. However, recent clinical revisions have suggested a potential correlation between cartilage degradation and intra-articular GCs, prompting clinicians to reconsider the effectiveness of this practice and evaluate alternative solutions [3]. As a result, alternative anti-inflammatory agents, including cytokine inhibitors, non-steroidal anti-inflammatory drugs, and naturally-derived anti-inflammatory molecules, have been investigated to address the cartilage pro-inflammatory conditions [4].

One such natural anti-inflammatory substance is the oleogum resin of *Boswellia serrata*, which has been used for centuries in traditional medicine. Over the past few decades, numerous *in vitro* investigations and studies involving human subjects have confirmed the potential of *Boswellia serrata* extracts (BSE) for treating various inflammatory diseases [5–7]. BSE is composed mainly of pentacyclic triterpenes known as boswellic acids (BAs), which possess biological activity and offer pharmacological actions [8]. The anti-inflammatory properties of BAs in different biological models can be associated to their molecular structures, which resemble glucocorticoids and act by suppressing the release of pro-inflammatory cytokines. Several authors have demonstrated that oral supplementation with BSE can prevent articular cartilage degradation, resulting in reduced pain in osteoarthritis patients [5,9]. On the other hand, the limited water solubility of BSE components hinders their use in regenerative medicine.

In this study, we present, for the first time, the preparation of a gellan gum-based hydrogel embedding BSE-loaded clay for *in situ* prevention of inflammatory disease with a potential application in cartilage tissue engineering. Gellan gum (GG) was selected for its attractive properties in cartilage regeneration, including high biocompatibility, low cytotoxicity, and a structure cartilage-like due to the presence of glucuronic acid residues [10]. Our previous studies have demonstrated the biocompatibility and chondrogenic support of different GG-based hydrogels reinforced with inorganic clays and active molecules [11–15].

MgAl-layered double hydroxides (LDH) clays were exploited for loading and *in situ* delivery of hydrophobic BSE in the gellan network. LDH has found fascinating applications in tissue engineering and drug delivery systems due to its layered channels with drug-carrying capacity, slow-release properties, good biocompatibility and biodegradability [16,17]. Recently, LDH-based systems have also shown promise in bone and cartilage repair [18,19].

In this study, pristine and calcined clays (coded as LDH and LDHc, respectively) were used to create systems with different BSE loading capacity, release, and biological performances [20]. The scaffold composition was carefully designed, embedding LDH-BSE or LDHc-BSE composites within a mixture of two types of gellan gum, one with high and one with low acyl content. This formulation aimed to create a biomaterial for cartilage regeneration with suitable anti-inflammatory and biomechanical performances. An extensive evaluation of the release profile of BAs from GG_{HL}/LDH-BSE and GG_{HL}/LDHc-BSE systems, along with a weight loss test, was carried out in a simulated synovial fluid. Moreover, we explored correlations between the hydrogels' mechanical and biological properties, focusing on the enhancement of chondrogenesis and reduction of the inflammatory response.

We hypothesized that the loading of BSE-containing composites into the carbohydrate network provides suitable mechanical and anti-inflammatory properties, enabling the up-regulation of anti-inflammatory pathways and related proteins. This may preserve the differentiation of stem cells into a cartilage-like phenotype, even under oxidative stress conditions.

Table 1
Composition (expressed as weight percent on the total weight of the components of the scaffold) of the prepared materials.

Scaffold code	Weight percent (%)				
	GG_H	GG_L	LDH or LDHc	LDH- or LDHc-BSE	BSE
GG_{HL}	60.0	40.0	–	–	–
GG_{HL}/BSE	48.0	32.0	–	–	20.0
GG_{HL}/LDH	48.0	32.0	20.0	–	–
GG_{HL}/LDHc	48.0	32.0	20.0	–	–
GG_{HL}/LDH-BSE	48.0	32.0	–	20.0	–
GG_{HL}/LDHc-BSE	48.0	32.0	–	20.0	–

2. Materials and methods

2.1. Materials

Hydrotalcite synthetic (magnesium aluminum hydroxycarbonate, CAS 11097–59-9, molecular weight 603.98 g/mol) – coded as LDH – and low acyl content gellan gum (Phytagel™, molecular weight 1×10^6 g/mol) – coded as GG_L – have been purchased from Sigma-Aldrich (Merck, Milan, Italy). High acyl content gellan gum (KELCOGEL® LT100, molecular weight $1–2 \times 10^6$ g/mol) – coded as GG_H – was supplied by CP Kelco (Atlanta, USA). The magnesium chloride salt, exploited as crosslinker, is of Redi-dri™ grade. *Boswellia Serrata* powder extract (containing 65 % boswellic acids, CAS 97952–72-2) – coded as BSE – was purchased from Farmalabor S.p.A. (Apulia, Italy). Hydrogel scaffolds have been prepared with ultrapure water, obtained through a Milli-Q® distillation system (Millipore-Merck, Darmstadt, Germany). All solvents and reagents have been purchased from Sigma Aldrich (Merck, Milan, Italy), unless otherwise specified.

2.2. Scaffold preparation

The formulation of the scaffolds has been based on a previously optimized GG_H and GG_L ratio [15]. Briefly, GG_H and GG_L have been dissolved in hot water (60 °C) at 1.2 % and 0.8 % *w/v* (GG_H:GG_L equal to 3:2), respectively. LDH has been used as received or calcined at 450 °C for 2 h (LDHc). Details on the calcination process of LDH and on preparation of LDH- or LDHc-BSE hybrid composites were reported elsewhere [20]. Briefly, the loading of BSE was achieved by equilibrating LDH with a 0.05 M BSE solution water/ethanol (25/75 *v*/v), for 24 h at room temperature. The recovered solid, obtained by filtration, was washed three times with distilled water and then dried at 60 °C until a constant weight was reached. Loading procedure for LDHc was the same used for the non-calcined clay, but replacing water with CO_2-free deionized water. The amount of LDH or LDHc added to the GG_{HL}-solution was based on a previously reported study on the influence of clays on the mechanical performances of the GG-based scaffolds [13]. BSE was also directly added to a solution containing GG_H and GG_L to obtain the GG_{HL}/BSE hydrogel. Hydrogels have been poured into 24-well plates (Flat bottom, Corning Inc., NY, USA) and crosslinked with magnesium ions [12]. For chemical characterizations, when dried samples are needed, the hydrogels have been frozen for 24 h (−20 °C), then freeze-dried at −55 °C for 24 h using an ALPHA 1–2 LD Plus freeze-drier (Martin-Christ, Osterode, Germany). In Table 1, a summary of the different hydrogels prepared is reported.

2.3. Physico-chemical and morphological characterization of the hydrogel

2.3.1. X-ray photoelectron spectroscopy (XPS)

The prepared hydrogels, once freeze-dried, have been sectioned and examined by means of XPS (PHI 5000 VersaProbe II, MN, USA). Analyses have been performed in high power mode with an AlKα X-ray radiation source and an instrument base pressure of 10^{-9} mbar. Wide scans and high-resolution scans have been recorded in fixed analyzer

transmission (pass energy of 117.4 eV and 29.35 eV, respectively). The MultiPak software (v.9.9.0.8) has been used for data mining, setting the reference charge to 284.8 eV (hydrocarbon peak).

2.3.2. Fourier-transform infrared spectroscopy (FT-IR) in attenuated total reflectance mode (ATR)

Freeze-dried samples were analyzed by means of FT-IR (ATR) analyses through a Spectrum Two PE instrument supplied by PerkinElmer, endowed with a universal ATR accessory (UATR, Single Reflection Diamond/ZnSe). For each of the relevant samples, FT-IR/ATR spectra were recorded from 400 to 4000 cm^{-1} with a 4 cm^{-1} resolution.

2.3.3. Thermo-gravimetric analysis (TGA)

The thermal behavior of the dehydrated hydrogels has been assessed by a PerkinElmer TGA-400 instrument (Perkin Elmer, Milan, Italy), heating 5–10 mg of the samples in the range 30–600 °C. The analyses have been performed in nitrogen, with a gas flow set at 20 mL/min. Data have been recorded by means of the TGA Pyris software (version 13.3.1.0014).

2.3.4. Morphological characterization

Scaffolds' morphology and porosity were visually investigated by Scanning Electron Microscopy (SEM, JSM-IT500 InTouchScope™ series, JEOL, Akishima, Japan) at accelerating voltage of 15 kV. The samples were fixed on aluminum stubs using carbon tape and gold-coated using a JEOL Sputter Coater machine (Smart coater from Jeol). The SmartView™ software (from Jeol) was used to calculate sample porosity, considering at least 20 random pores obtained from 3 SEM images of the same specimens. The void area percentage was calculated as the percentage ratio of total pore area to the total area as previously reported by the Authors [13].

2.4. Evaluation of the release of Boswellic acids from GG_{HL}/LDH-BSE and GG_{HL}/LDHc-BSE systems

Two experiments were carried out for the qualitative and semi-quantitative evaluation of the release of BAs from GG_{HL}/LDH-BSE and GG_{HL}/LDHc-BSE systems into a simulating synovial fluid solution [14,21] containing ethanol at 10 % v/v (SSFE).

For each of the two experiments, triplicates of GG_{HL}/LDH-BSE and GG_{HL}/LDHc-BSE systems were prepared and the resulting cylinders showed an average mass of 2.55 ± 0.18 g. Each cylinder was immersed in 5 mL of SSFE.

The first experiment aimed at the determination of the release profile of BAs in SSFE. After 21 days, a 2 mL aliquot of the release medium (RM) was withdrawn and transferred into a 15 mL glass centrifuge tube. 2 mL of chloroform were added for the liquid-liquid extraction (LLE) of BAs from the RM. The resulting system was vigorously stirred using a vortex mixer. A stable phase separation was reached after centrifugation (4500 rpm) for 10 min. 1 mL of the chloroform-rich phase was recovered and subjected to solvent evaporation under controlled nitrogen flux. The dry residue was re-dissolved in pure methanol prior to its characterization by reversed-phase chromatography (RPLC) coupled to electrospray ionization (ESI) high-resolution mass-spectrometry (HRMS). Further information about the RPLC-ESI-FTMS instrumentation and operating conditions are reported in Section S1.2 (see Supplementary material).

The second experiment was focused on the determination of the transfer kinetics of the 11-keto-β-boswellic acid (β-KBA) from GGHL/LDH-BSE and GGHL/LDHc-BSE into the SSFE medium. Indeed, β-KBA was found to be predominantly released in SSFE in respect to the other BAs enclosed in the LDH-BSE and LDHc-BSE composites (see Section 3.2 for further details). Unlike other BAs, both β-KBA and its acetylated form, *i.e.*, the 3-acetyl 11-keto-β-boswellic acid (β-AKBA), exhibit a distinctive absorption peak in the UV region at 250 nm [22]. Hence, a simpler analytical approach based on reversed-phase liquid chromatography, coupled with UV detection was exploited for monitoring the release kinetics of β-KBA in SSFE. Details about the RPLC-UV instrumentation and operating conditions are described in Section S1.3 (see Supplementary material). For each of the three cylinders of GG_{HL}/LDH-BSE and GG_{HL}/LDHc-BSE immersed in SFFE, a 500 μL volume of the RM was withdrawn after 1, 2, 7, 12 and 21 days. After each withdrawal, the remaining volume of the RM was readily integrated by the addition of 500 μL of fresh SSFE. The collected RM samples were filtered using 0.45 μm PTFE filters prior to the RPLC-UV analysis. The released amount of β-KBA was estimated as described in Section S1.4 (see Supplementary material).

2.5. Mechanical characterization of the hydrogels

The UniVert Test Device UV-200-01 (CellScale, Waterloo, Canada) was utilized to analyze the prepared hydrogels through compression tests. The samples ($n = 5$) had a diameter of approximately 16 mm and a height of about 20 mm, which were prepared in advance in 24-multiwell plates. The compression tests were conducted at a crosshead speed of 2.5 mm/min, and the load was applied until the point of fracture was reached [15]. The compressive modulus was determined by calculating the slope of the initial linear portion of the stress-strain curve (0–10 %). Additionally, the strain at break values was calculated.

Rheological tests were conducted using the MCR302e stress-controlled rheometer (Anton Paar GmbH, Graz, Austria), equipped with a Taylor-Couette geometry (concentric cylinder geometry). The inner diameter of the cylinder was 16.662 mm, and the gap between the cylinders was set to 0.504 mm. Specifically, a frequency sweep test was performed, covering a range of angular frequencies (ω) from 100 to 0.1 rad/s, while maintaining a strain value of 1 % within the linear viscoelastic region. To ensure accuracy and consistency, these rheological tests were carried out in triplicate. Throughout each test, the temperature was maintained at 21 °C using a Peltier system as a control parameter.

2.6. Biological evaluation

2.6.1. Cells

A well-established cell line of Human mesenchymal stromal cells (hMSC) immortalized by hTERT lentiviral vector [23] was used for cytocompatibility and chondrogenic evaluations. Cells were cultured using low-glucose Dulbecco's Modified Minimal Essential Medium (DMEM-LG, form ThermoFisher) supplemented with 15 % fetal bovine serum (FBS) and 1 % penicillin/streptomycin (PS) and maintained at 37 °C and 5 % CO_2. Once cells' confluency reached 85–90 %, cells have been detached by 0.25 % trypsin/EDTA solution, harvested, and used for the experiment.

2.6.2. Scaffolds' cytocompatibility

In order to test composites' cytocompatibility and cells' distribution within pores, cylindrical specimens (5 mm height – 8 mm diameter) have been used to realize 3D cultures resembling tissue ingrowth as previously reported by the Authors [12,14,15]. Briefly, 3×10^6 cells/scaffold have been mixed into collagen hydrogel (PureCol EZ Gel solution, type I collagen, 5 mg/mL, from Merck) that was used as temporary substrate and gently dropwise seeded into the composites; then, cells-colonized scaffolds were firstly incubated 2 h at 37 °C to allow complete collagen gelation and subsequently submerged with 2 mL of medium. Specimens' cytocompatibility was verified by means of the colorimetric metabolic assay Alamar blue (High sensitivity AlamarBlue, from Thermo Fisher, 0.015 % in DMEM-LG) where the conversion of the non-fluorescent molecule resazurin into the fluorescent molecule resorufin occurs only for metabolically active viable cells; fluorescence was recorded at 590 nm using a spectrophotometer (Spark, from Tecan) and results were expressed as relative fluorescent units (RFU). After 72 h cultivation in 3D conditions, the viability of the cells as well as their distribution within composites' pores were visually checked by the

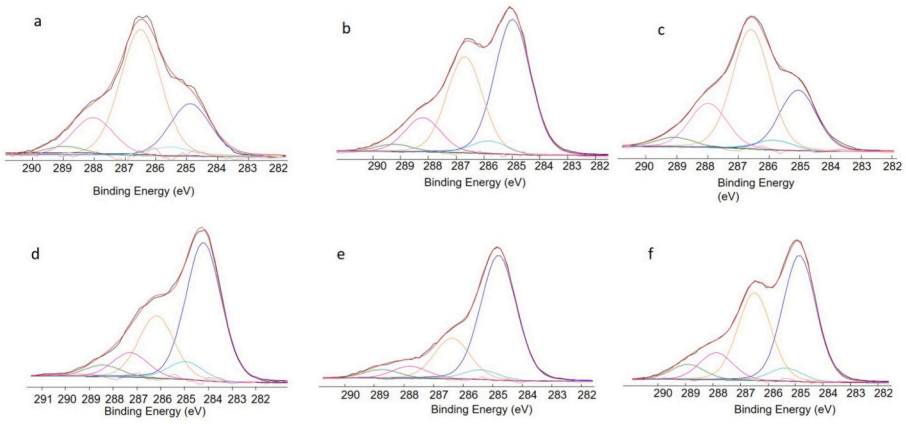

g

Sample	Atomic percentage (%)					CHx/O-C-O (or C=O)	COOR/O-C-O (or C=O)
	CHx 284.8 eV	C-COOR 285.5 eV	C-OR 286.4 eV	O-C-O (or C=O) 288.0 eV	COOR 288.8 eV		
GG_{HL}	30.0	3.7	43.1	20.1	3.1	1.5	0.2
GG_{HL}/BSE	54.5	6.9	24.4	9.6	4.5	5.7	0.5
GG_{HL}/LDH	47.2	4.5	33.6	12.0	2.7	3.9	0.2
GG_{HL}/LDH-BSE	63.6	4.8	20.8	6.3	4.5	10.0	0.7
GG_{HL}/LDHc	26.0	4.0	49.1	18.2	3.8	1.4	0.2
GG_{HL}/LDHc-BSE	46.9	5.0	32.5	10.1	5.5	4.6	0.5

Fig. 1. Curve fitting of C1s high-resolution spectra relevant to: a) GG_{HL}, b) GG_{HL}/LDH, c) GG_{HL}/LDHc, d) GG_{HL}/BSE, e) GG_{HL}/LDH-BSE and f) GG_{HL}/LDHc-BSE. Peaks attribution (BE) and atomic percentages (%) of all the C1s curve-fittings are reported in g). The maximum error on the binding energy values was equal to +0.2 eV.

fluorescent live/dead assay (Live/Dead ready-to-use kit from Thermo Fischer) using a confocal microscope (TCS SP8 LIGHTNING, Leica Microsystems). To quantify the number of viable cells/are, confocal images were further analyzed by the particle analyzer plug-in of the ImageJ software (imposed limit = particles >15 mm).

2.6.3. Anti-inflammatory evaluation

In order to assess whether BSE enriched materials can modulate the inflammatory process by acting as scavenger, a pro-inflammatory environment was chemically induced *via* oxidative stress. Accordingly, H_2O_2 (300 μM) was introduced into the medium used to cultivate the 3D models detailed in 2.6.2 with a regime of 6 h/day for 7 days in order to generate toxic oxygen species (ROS) [14]; afterwards, RNA extraction was performed using TRIzol reagent (from Invitrogen) while cDNA was synthesized using the iScript gDNA Clear cDNA Synthesis Kit (from Bio-Rad Laboratories). Real-time PCR was run with the SsoAdvanced Universal SYBR Green Supermix (Bio-Rad Laboratories) to detect the expression of the pro/anti-inflammatory genes Prostaglandin E Synthase 2 (PGE2), Cyclooxygenase 2 (COX2), Interleukin 1 Beta (Il1β) and Interleukin 6 (Il6). For data analysis, the fold change of each gene expression was calculated using the $2^{-\Delta\Delta Ct}$ method, considering the Glyceraldehyde-3-phosphate dehydrogenase (GAPDH) as housekeeping gene to normalize the results. Primers and probes are detailed in the Supplementary Table S3.

2.6.4. Chondrogenesis

The cellularized 3D composites were prepared as described in Section 2.6.2 and equilibrated for 24 h in a maintenance medium (DMEM-LG 15%FBS) to allow complete cells adhesion and spread into the collagen matrix. Afterward, the maintenance medium was removed and replaced by the chondrogenic one composed of DMEM High Glucose (4.5 g/L), 10 % ITS+1 Premix Tissue Culture Supplement, 10^{-7} M dexamethasone, 1 μM ascorbate-2-phosphate, 1 % sodium pyruvate, and 10 ng/mL transforming growth factor-beta 1 (Tgf-β1) [12,14]. Composites were maintained in the chondrogenic medium for 21 days with medium changed every 3 days; afterwards, RNA was extracted and cDNA was synthesized to run real-time PCR as previously detailed in 2.6.3. Chondrogenic genes collagen type II (COL 2), aggrecan (ACAN), and SRY-Box Transcription Factor 9 (SOX 9) expression was evaluated to demonstrate the ability of the composited to support hMSC differentiation towards the chondrocytes-like genotype. Moreover, to confirm the ability of the BSE-loaded scaffolds to modulate the expression of pro-inflammatory genes up-regulated by the stimuli induced by the Tgf-β1 during chondrogenesis, the expression of the pro/anti-inflammatory genes Prostaglandin E Synthase 2 (PGE2), Interleukin 10 (IL10), and Tumor necrosis Factor alpha (TNFα) has been evaluated.

For data analysis, the fold change of each gene expression was calculated using the $2^{-\Delta\Delta Ct}$ method, considering the Glyceraldehyde-3-phosphate dehydrogenase (GAPDH) as housekeeping gene to normalize the results. Primers and probes are detailed in the Supplementary Table S4.

Finally, the presence of cartilage-like collagen type 2 was visually checked by immunofluorescence after 21 days differentiation; specimens were washed 3 times with PBS, permeabilized with 0.5 % Triton-X 100 (Thermo Fisher) in PBS for 30 min, and incubated in blocking solution (1 % BSA, 22.52 mg/mL glycine in PBST consisting of Phosphate-Buffered Saline +0.1 % Tween® 20 Detergent) to prevent non-specific binding of the primary antibody. A solution containing the primary antibody Anti-collagen II (1:500 in PBS + 1 % BSA, Abcam) was incubated overnight at 4 °C on an orbital shaker. After washing with PBS, a specific secondary antibody (Alexa Fluor 647, 1:500 in PBS + 1 % BSA) was applied and maintained for 1 h at room temperature with gentle oscillation. Counterstaining was performed with 4′,6-diamidino-2-phenylindole (DAPI), diluted 1:1000 in PBS + 1 % BSA. Samples were observed using the THUNDER fluorescent microscope (Leica).

2.6.5. Proteomics analysis

To confirm results from the gene expression at the proteins level, proteomics was applied. In order to rank the ability of the scaffolds to properly support chondrogenesis as well as to reduce the pro-inflammatory cascade, hMSC cultivated in basal medium (named as Basal) were included in the experiments to set-up the starting conditions; accordingly, cellularized constructs induced towards chondrogenesis were compared firstly to the Basal group to confirm the cartilage-like maturation and then match to each other with the aim to clarify the contribute of the BSE. The total amount of proteins was

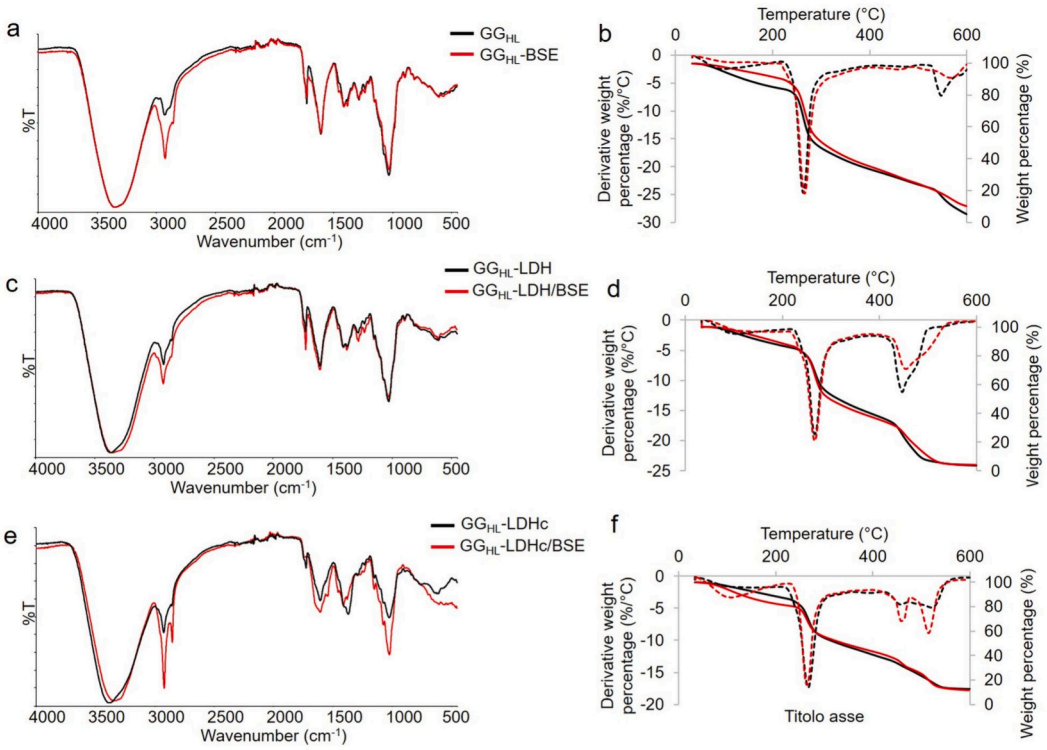

g

Sample	Water/volatiles (%)	T_1/weight loss (°C/%)	T_2/weight loss (°C/%)	T_3/weight loss (°C/%)	Residue at 600°C (%)
GG$_{HL}$	15.5	263.7/50.5	547.1/13.5	585.2/4.5	5.1
GG$_{HL}$/BSE	7.1	266.2/57.8	523.4/5.8	567.6/9.6	10.2
GG$_{HL}$/LDH	12.0	267.3/45.3	447.2/22.2	470.4/15.1	3.5
GG$_{HL}$/LDH-BSE	12	267.4/49.0	454.6/21.6	484.5/13.1	4.0
GG$_{HL}$/LDHc	15.7	263.5/31.6	446.6/9.7	542.2/13.2	12.8
GG$_{HL}$/LDHc-BSE	20.6	263.5/36.5	459.1.3/19.7	515.3/17.7	11.6

Fig. 2. FT-IR/ATR (a, c and e) spectra comparison and TGA (solid lines)/DTGA (dotted lines) traces (b, d and f) of GG$_{HL}$ and GG$_{HL}$/BSE (a, b), GG$_{HL}$/LDH and GG$_{HL}$/LDH-BSE (c, d) and GG$_{HL}$/LDHc and GG$_{HL}$/LDHc-BSE (e, f). In panel (g) were reported water/volatiles content, thermal degradation steps and residue at 600 °C of all the investigated systems.

obtained after sample homogenization in RIPA buffer, and further sonicated. Proteins were then precipitated with cold acetone and resuspended. Proteins were then reduced in 25 μL of 100 mM NH4HCO3 with 2.5 μL of 200 mM DTT (Merck) at 60 °C for 45 min and next alkylated with 10 μL 200 mM iodoacetamide (Merck) for 1 h at RT in dark conditions. Iodoacetamide excess was removed by the addition of 200 mM DTT. Proteins were digested with trypsin. The digests were dried by Speed Vacuum and then desalted. Digested peptides were analyzed on an Ultimate 3000 RSLC nano coupled directly to an Orbitrap Exploris 480 with a High-Field Asymmetric Waveform Ion Mobility Spectrometry System (FAIMS) (all Thermo Fisher Scientific). The false discovery rate (FDR) was set to 1 %. Statistical analyses and *t*-test were performed on protein abundances using MetaboAnalyst software. The details of the machine set-up are reported in the Supplementary file S1.5.

2.7. Statistical analyses of data

Biological experiments were carried out using six sample replicates. Statistical analysis of data was performed using the SPSS software (v.20.0, IBM). Data were compared by ANOVA, followed by Tukey's test. The significance level was set at $p < 0.05$.

3. Results and discussion

3.1. Physicochemical and morphological characterization of the hydrogels

3.1.1. X-ray photoelectron spectroscopy (XPS)

XPS analysis was carried out to investigate the surface chemical composition of the carbohydrates/clay/vegetal extract composites. In particular, the deconvolution of the C1s spectra of GG$_{HL}$, GG$_{HL}$/BSE, GG$_{HL}$/LDH, GG$_{HL}$/LDH-BSE, GG$_{HL}$/LDHc and GG$_{HL}$/LDHc -BSE was reported in Fig. 1a–f and the relevant attributions and atomic percentages in Fig. 1g. The GG$_{HL}$ C1s curve fitting has been already reported [15] but, to allow a correct comparison with the other specimens, has been inserted in Fig. 1a. The addition of clay, *i.e.*, in GG$_{HL}$/LDH and GG$_{HL}$/LDHc samples (panels b and c), did not caused significant differences: in particular, the COOR/O-C-O (or C═O) ratio remained equal to about 0.2 as well as the binding energy values, suggesting that no interaction between clays and organic network occurred (see Fig. 1g). On the other hand, an increase of this ratio was recorded in all the BSE-containing samples (panels d, e and f); this feature could be ascribed to the presence of a high content in boswellic acids, bringing carboxylic acid groups, in the vegetal extract. Moreover, since BSE contains mainly

aliphatic and alkene groups, a huge increment of CHx/O-C-O (or C═O) ratio was observed when BSE was present, even if CHx peak was always affected by hydrocarbon contamination. Anyway, despite the presence of contamination, the latter ratio, as well as the COOR/O-C-O (or C═O) one, evidenced a clear BSE presence on the surface of the BSE-containing composites, thus allowing us to consider a prompt BSE availability for the cells, despite of their low solubility and release.

3.1.2. FT-IR/ATR analysis

FT-IR analysis, carried out in ATR mode (see Fig. 2a, c and e) on gellan gum-based hydrogel composites evidenced main absorption bands ascribable to low and high acyl gellan gums, as already reported in a previous work [15]. The presence of LDH and LDHc did not significantly change the FT-IR spectrum of the relevant composites, since the main clay's absorption bands, the broad band of hydroxyl groups of water and hydroxyl groups located between the layers at about 3419 cm^{-1} and the carbonate peak at 1366 cm^{-1} present in the LDH, overlapped with the polymer absorption bands.

On the other hand, the presence of BSE was revealed by the increment of alkyl C—H stretching at 2924 and 2859 cm^{-1}. Moreover, the carboxylic C═O bond ascribable to boswellic acids was evidenced by the absorption band 1699 cm^{-1}, less intense than the C═O relevant to GG_H acyl moieties falling at 1724 cm^{-1} [15]. Furthermore, the appearance of C═C bending at 1454 cm^{-1} and C=C–C=O stretching at 1241 cm^{-1} can be detected in all the BSE-containing systems [24,25]. On the other hand, a more significant change in FT-IR spectrum was observed in the GG_{HI}/LDHc-BSE system where the appearance of asymmetric and symmetric stretching of carboxylates, falling at 1549 and 1381 cm^{-1}, was detected as already reported [20].

3.1.3. Thermal characterization by TGA

TGA (solid lines) and DTGA (dotted lines) traces relevant to GG_{HL} and GG_{HL}/BSE, GG_{HI}/LDH and GG_{HL}/LDH-BSE, GG_{HL}/LDHc and GG_{HI}/LDHc-BSE samples are reported in Fig. 2b, d and f.

In GG_{HL} sample (Fig. 2b, black line), a moisture content of about 15.5 % was recorded. As known, carbohydrates possess high affinity for water [26,27] and three different kinds of water can be present in carbohydrate-based hydrogels, *i.e.*, free water (which was released already at 60 °C), hydrogen-bonds linked water (released in the range 80–120 °C) and water linked with electrostatic interaction with ionized groups of polymer (which evolved at temperatures up to 160 °C) [26,27]. Here, we considered overall water/volatiles release process, evaluating the weight loss up to 200 °C. The main decomposition peak ascribable to the polymer backbones fell at 263 °C, accompanied by lower and partially overlapped decomposition steps, at temperatures higher than 520 °C, with a residue at 600 °C of about 5 %. For GG_{HL}/BSE sample (Fig. 2b, red line), a lower moisture content (about 7 %) was recorded, probably due to the incorporation of a more hydrophobic backbone, such as BSE. The main polymers decomposition peak fell at 266 °C, accompanied by other two at higher temperatures, slightly anticipated respect to those of $GG_{HL,}$ with a final residue at 600 °C of about 10 %. As far as GG_{HI}/LDH is concerned (Fig. 2d, black line), a moisture content of 12 % was detected, and the main decomposition peak fell at 267 °C. The second and third decomposition steps were significantly anticipated, probably linked to the weight losses relevant to the clay [20]. The residue at 600 °C was about 4 %. In GG_{HL}/LDH-BSE (Fig. 2d, red line), a similar moisture content (12 %) was detected. The main decomposition peak was once again at 26 °C, while the two decomposition peaks fell at 454.5 and 484.5 °C, and a residue similar to the GG_{HL}/LDH sample was found. Finally, for GG_{HL}/LDHc and GG_{HL}/LDHc-BSE (Fig. 2f, black and red lines, respectively), a moisture content of 15.7 and 20.6 % was respectively detected. Only in this case, the presence of BSE incremented the moisture content, probably because a high amount of boswellic acids in their ionized form was present, as detected by FT-IR analysis. The main decomposition peak fell at 263.5 °C, for both GG_{HL}/LDHc and GG_{HL}/LDHc-BSE. In the case of the calcined clay-containing composites, the second and third decomposition steps were also anticipated respect to GG_{HL} and GG_{HL}-BSE. Concluding, for both these samples high residues at 600 °C were recorded, which can be related to the fact that the calcined clay presented a significantly higher residue than the native one [20]. All the temperatures and weight loss details were reported in Fig. 2g.

Table 2
Composites porosity evaluation. Results are reported as mean ± standard deviation on 20 values/composite.

	Void area %	Mean pore area (μm^2)	Mean pore diameter (μm)
GG_{HL}	37.9 ± 0.7	64,300 ± 1100	290 ± 90
GG_{HL}/BSE	48.2 ± 1.0	153,200 ± 1400	440 ± 110
GG_{HL}/LDH	24.7 ± 0.4	46,700 ± 900	240 ± 60
GG_{HL}/LDH-BSE	24.5 ± 0.5	45,900 ± 1100	240 ± 90
GG_{HL}/LDHc	34.9 ± 0.5	59,000 ± 2000	280 ± 180
GG_{HL}/LDHc-BSE	45.7 ± 0.9	130,000 ± 11,000	400 ± 200

3.1.4. Morphological characterization

Scanning Electron microscopy (SEM) imaging was used to investigate composites' morphology and to determine the size of the pores; based on these values, the total porosity and the void area were calculated. SEM images are reported in Fig. 4, while pores size, porosity and void area of each composites are summarized in the Table 2.

In general, all the samples showed a porous architecture, with "open-cell" structures, characterized by a high degree of interconnectivity, thus being suitable to host cells seeding in a 3D arrangement (Fig. 3).

As calculated from the SEM images (representative images are reported in the Supplementary Fig. S2), the mean pore diameter ranged from 290 (± 90) μm of the GG_{HL} specimens to the 440 (± 110) μm of the GG_{HL}/BSE ones. Moreover, the % of void area was measured to range from 24.5 ± 0.5 for GG_{HL}/LDH-BSE to 48.2 ± 1.0 for GG_{HL}/BSE as summarized in Table 2 below.

3.2. Characterization of the release profile of Boswellic acids from GG_{HL}/LDH-BSE and GG_{HL}/LDHc-BSE systems through RPLC-ESI-FTMS

From a chemical point of view, the oloeogum resin that is exudated from Boswellia trees is a complex mixture of polysaccharides and a large variety of terpenes and terpenoids [28,29]. Among the latter, boswellic acids (BAs) have been recognized as the major bioactive compounds in the resin [30]. Notably, a BAs-enriched *Boswellia Serrata* extract (BSE) was exploited to produce LDH-BSE and LDHc-BSE composites that were enclosed in the gellan gum-based systems. Consistently with data declared by the producer, BAs represented the 65 % of the BSE dry weight.

Both LDH-BSE and LDHc-BSE were deeply investigated in our previous work [20]. Despite the two systems exhibited a comparable content of the most hydrophilic BA, *i.e.*, 11-keto-β-boswellic acid (β-KBA), the LDHc-BSE composite showed a higher loading yield for the most hydrophobic BAs (*e.g.*, α-boswellic acid, β-boswellic acid and the corresponding acetylated forms). Hence, the calcination process was proven to generally enhance the loading of BAs [20]. On the other hand, conversely to what observed for LDH-BSE composites, the quantitative methanol-based extraction of the loaded amount of BA from the LDHc-BSE system required the chemical disruption of the inorganic matrix, thus indicating a stronger chemical interaction between the BAs and LDHc [20]. For all these reasons, both LDH-BSE and LDHc-BSE composites were considered of interest for the production gellan gum-based systems.

The interest in BAs was motivated by their well-known anti-inflammatory properties [31–33]. Specifically, 11-keto-β-boswellic acid and the 3-acetyl 9,11-dehydro-β-boswellic acid (β-AKBA) were recognized as

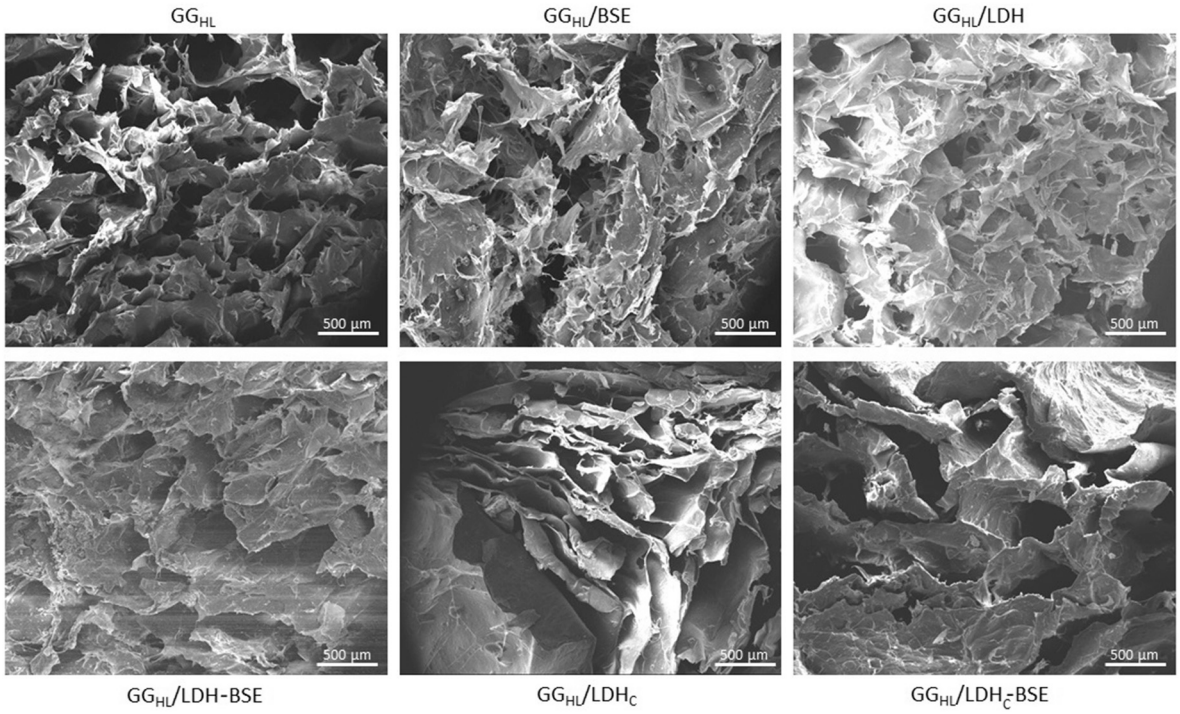

Fig. 3. Composites morphological analysis.

powerful noncompetitive inhibitor of the 5-lipoxigenase, *i.e.*, the key enzyme involved in the biosynthesis of leukotrienes [34,35]. The presence of both β-KBA and β-AKBA in the LDHc-BSE composites has been previously assessed in our previous work [20], along with 4 more BAs, namely α-boswellic acid (α-BA), β-boswellic acid (β-BA), 3-acetyl α-boswellic acid (α-ABA), and 3-acetyl β-boswellic acid (β-ABA). Additionally, the hyphenation of reversed-phase liquid chromatography (RPLC) with electrospray ionization (ESI) high-resolution Fourier-Transform mass spectrometry (FTMS) allowed us to recognize up to 7 isomers for α and-β BA and 4 more isomers for the corresponding acetylated forms (*i.e.*, α-ABA and β-ABA). Notably, the majority of the of the peaks detected in the total ion current chromatogram (TICC) shown in Fig. S3 could be attributed to $[M-H]^-$ ions of the BAs of interest and their isomers, thus confirming their predominance in the chemical composition of BSE. Analogously to what we did in our previous manuscript [20], we will not consider the first two eluting isomers of α-BA and β-BA due to their very low abundance in BSE. We will also adopt an analogous nomenclature based on the elution order on a C18 stationary phase, thus referring to α and β-BA isomers as: BA isomer 3, BA isomer 4, BA isomer 5, BA isomer 6, and BA isomer 7. Similarly, α-ABA and β-ABA isomers will be coded as ABA isomer 1, ABA isomer 2, ABA isomer 3, and ABA isomer 4.

The water solubility of BAs is extremely low [36]. Nevertheless, in our previous work [20], we observed that β-KBA was preferentially released in a phosphate-buffered saline (PBS) solution (pH 7.4) in respect to the other BAs embedded in the LDH-BSE and LDHc-BSE composites. Hence, we decided to assess whether a similar release profile could be observed after 21 days of immersion of GG$_{HL}$/LDH-BSE and GG$_{HL}$/LDHc-BSE into the ethanol enriched simulating synovial fluid (SSFE). An analogous computational approach to the one described by Cometa et al. [20] was adopted for the determination of the release profile. Specifically, the contribution of each BA to the release profile was calculated as the percent ratio between the extracted ion current chromatogram (EIC) peak area of the BA of interest, and the sum of the EIC peak area calculated for all the BAs enclosed in the LDH-BSE and LDHc-BSE composites. The extraction of the ion current was performed using a very narrow *m/z* window (5 ppm) centered on the theoretical mass of the $[M-H]^-$ ion of the analyte of interest. The calculated values were compared with those observed for the BAs profile observed in pure BSE. The latter were calculated after the RPLC-ESI(−)-FTMS analysis of methanol solutions containing BSE at 0.1, 1 and 5 μg/mL. The computed relative abundances are shown in Table S2 (see Supplementary material) and graphically displayed in Fig. 4. In the case of GG$_{HL}$/LDH-BSE and GG$_{HL}$/LDHc-BSE, the values in Table S2 refer to triplicates of the first release experiment described in Section 2.4. As can be inferred from Fig. 4, β-KBA was preferentially released in SSFE in respect to the other BAs and their isomers. This is consistent with the higher polarity of β-KBA in respect to the other analytes of interest for this study. Indeed, β-KBA was the first species to be eluted when a C18 stationary phase was adopted [20].

Concluding, even if the total BAs loading in LDHc-BSE was higher than in LDH-BSE, the composition of the BAs released from GG$_{HL}$/LDH-BSE and GG$_{HL}$/LDHc-BSE was not significantly different.

3.3. Determination of the release kinetics of 11-keto-β-boswellic acid from GG$_{HL}$/LDH-BSE and GG$_{HL}$/LDHc-BSE systems based on RPLC-UV

As stated in Section 3.2, β-KBA was found to be predominantly released from both GG$_{HL}$/LDH-BSE and GG$_{HL}$/LDHc-BSE cylinders after 21 days of immersion in SSFE. Hence, we decided to further investigate the release kinetics of β-KBA. To such purpose, a simpler RPLC method than the one exploited for the determination of the release profile (see Section S1.2, Supplementary material) was adopted. It was based on an isocratic elution coupled to UV detection, as described in Section S1.3 (see Supplementary material). Notably, both β-KBA and its acetylated form (*i.e.*, β-AKBA) exhibit very similar UV–Vis spectra. However, as reported in our previous work [20], the correct attribution of the signals pertaining to β-KBA and β-AKBA was achieved through the alignment of the RPLC-UV trace acquired at 250 nm (see Fig. S4B, Supplementary material), and the RPLC-ESI(−)-FTMS extracted ion chromatograms (EIC) related to the $[M-H]^-$ ions of β-KBA (*m/z* 469.3323) and β-AKBA (*m/z* 511.3429) (Fig. S4A, Supplementary material). Thereafter, the elution order and the relative intensities of the RPLC-UV signals observed for β-KBA and β-AKBA using the multi-step elution gradient

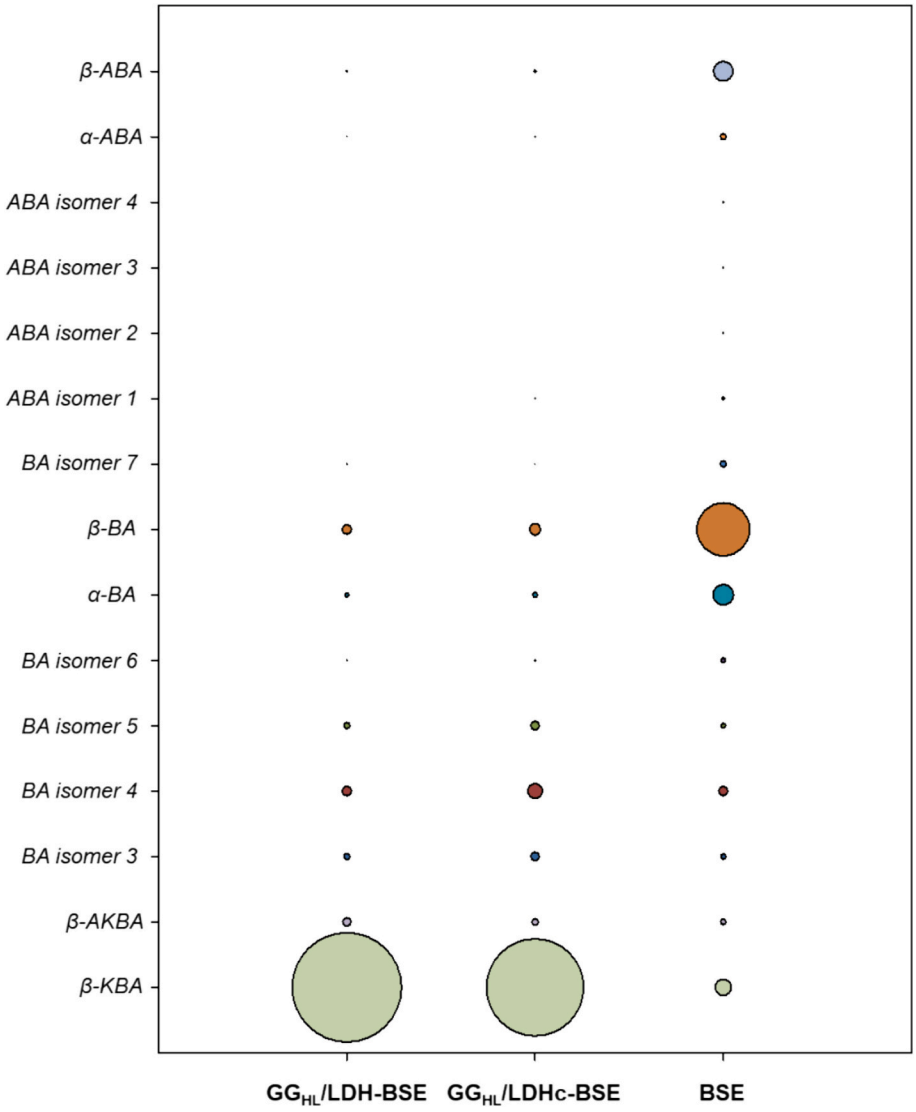

Fig. 4. Bubble plot displaying the comparison between the release profile in SSFE of BAs from GG_{HL}/LDH-BSE and GG_{HL}/LDHc-BSE systems, and the BAs profile in pure BSE. The bubble area is proportional to the relative abundances shown in Table S2 (see Supplementary material). The latter were calculated from the EIC peak area values obtained for each analyte, as described in Section 3.2.

described in Section S1.2 (see Supplementary material) was exploited for identifying the corresponding peaks in the RPLC-UV trace (see Fig. S4C, Supplementary material) recorded with the isocratic elution method described in Section S1.3 (see Supplementary material).

Fig. 5 displays the graphical outcome for the release kinetics of β-KBA from GG_{HL}/LDH-BSE and GG_{HL}/LDHc-BSE in SSFE. The technical details related to the release experiment were discussed in Section 2.4. Interestingly, similar release kinetics were observed for β-KBA from GG_{HL}/LDH-BSE and GG_{HL}/LDHc-BSE in SSFE. In both cases, a comparable plateau seems to be between 12 and 21 days of contact with the release medium. The similar behavior of the two systems is also consistent with our previous findings [20] about the β-KBA loading of LDH-BSE and LDHc-BSE systems. Finally, GG_{HL}-BSE system showed a burst β-KBA release (data not shown), differently from what observed on systems containing LDH or LDHc as BSE carriers, which conversely evidenced a controlled BSE release over time.

3.4. Mechanical characterization of the hydrogel

Fig. 6a displays a representative stress-strain curve obtained after performing static compression test on the sample GG_{HL}/LDHc-BSE. All the samples showed similar behavior with an initial elastic region (up to 10–15 % of the strain), followed by a densification regime, likely due to the closer proximity between the polymer chains under complete compression, resulting in a rapid increase in stress [37]. Mechanical properties such as the elastic modulus and strain at break can be calculated from these stress-strain curves. These values have been reported in Fig. 6b. All the hydrogel formulations containing LDH, with or without BSE, resulted in a three-fold increase in the compressive Young's modulus ($p < 0.001$) compared with the bare GG_{HL} samples, with values of 110 ± 15 kPa for GG_{HL}/LDHc-BSE and 60 ± 20 kPa for GG_{HL}/BSE. The observed enhancement in mechanical properties can be attributed to the clay, which is capable of forming networks within the polymeric hydrogel formulation. This is consistent with our previous paper, where the addition of inorganic clays to gellan gum and Manuka honey-based hydrogels increased the Young's modulus by at least 40 % compared to the bare polymeric formulation [13]. The values measured for the clay-reinforced hydrogels are higher or fall within the range of compressive properties reported for gel formulations proposed for cartilage regeneration [38,39]. It is worth noting that no statistical differences were observed between the samples containing LDH, whether subjected to calcination or not ($p > 0.05$), and whether with or

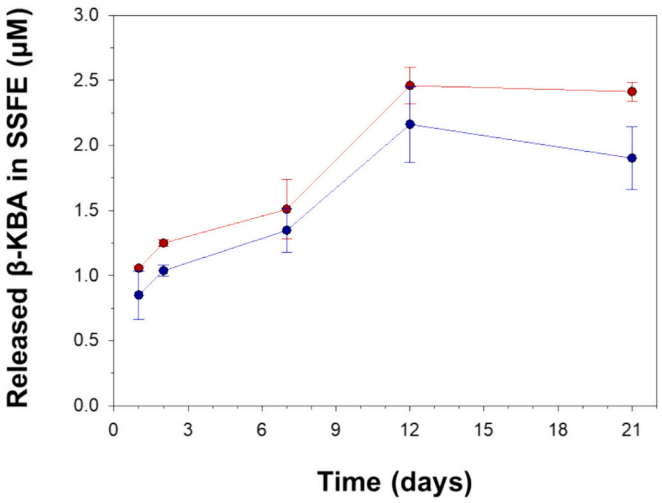

Fig. 5. Line and scatter plot showing the release kinetics of β-KBA in SSFE from GG_{HL}/LDH-BSE (blue color) and GG_{HL}/LDHc-BSE (red color). The error bars are representative for the standard deviation values calculated for triplicates of the release experiment (see Sections 2.5 and S1.4 for further details).

without BSE. Furthermore, all the clay-reinforced hydrogels showed higher values of strain at break, reaching a maximum value of 40 ± 3 % in the sample GG_{HL}/LDHc-BSE compared with the unloaded hydrogels (30 ± 3 % and 29 ± 2 % for GG_{HL} and GG_{HL}/BSE respectively), resulting in an increased elastic deformability of the hydrogels. Indeed, this characteristic is particularly important for soft tissue engineering applications like cartilage, skin, and arterial tissues, where high deformability is required [40,41]. To mimic the properties of natural tissues, artificial tissues or scaffolds need to possess the ability to retain elastic recovery, ensuring that they can bounce back to their original shape after undergoing deformation [42].

Moreover, to assess additional mechanical properties of the polymeric networks, we employed a rheometer to apply shear stress to the hydrogels. Fig. 7 illustrates the characteristic relationship between the storage modulus (G′) and the loss modulus (G″) as a function of oscillation stress for all the prepared hydrogels. Specifically, the frequency sweep test was used to establish the correlation between the testing frequency and the storage and loss moduli of a substance. Additionally, it provides insight into the viscoelastic characteristics and condition of a material by comparing the G′ and G″ values across a range of frequencies [43]. In this work, for all oscillation stress levels, the storage modulus (G′) surpassed the loss modulus (G″), indicating the gel-like behavior of the material. This observation suggests that all the prepared hydrogels exhibit a solid-like nature, with the ability to store and recover energy [44]. Furthermore, no crossover point between the storage and loss modulus was detected across the examined frequencies, indicating that all the hydrogels possessed interconnected fibrous networks. Unlike what was observed in the static compression tests, all the hydrogels containing BSE presented higher G′ values, reaching 4050 ± 40 kPa at 1 Hz for the GG_{HL}/LDHc-BSE sample compared to 1018 ± 14 kPa for the GG_{HL}/LDHc sample. This indicates that the addition of BSE resulted in a stronger and more cohesive intermolecular network formed through polysaccharide interactions as suggested by Yu et al. for the development of 3D food printing inks [45].

3.5. Biological evaluations

3.5.1. Cytocompatibility

Due to the novelty of the composites presented here, the first step involved demonstrating their cytocompatibility by verifying the presence of viable cells seeded in 3D within the pores. This was assessed through their metabolic activity over a 3-day culture period by verifying the metabolic activity of viable cells being able to convert into a fluorescent dye the alamar blue reagent. Results are reported in Fig. 8. In general, all the BSE-loaded LDH composites (GG_{HL}/LDH-BSE, GG_{HL}/LDHc-BSE) reported the presence of metabolically active cells in a comparable manner to the unloaded GG_{HL} controls (Fig. 8a, $p > 0.05$); conversely, the composites loaded with the free BSE (GG_{HL}/BSE) reported a decreased metabolic activity in comparison to both controls

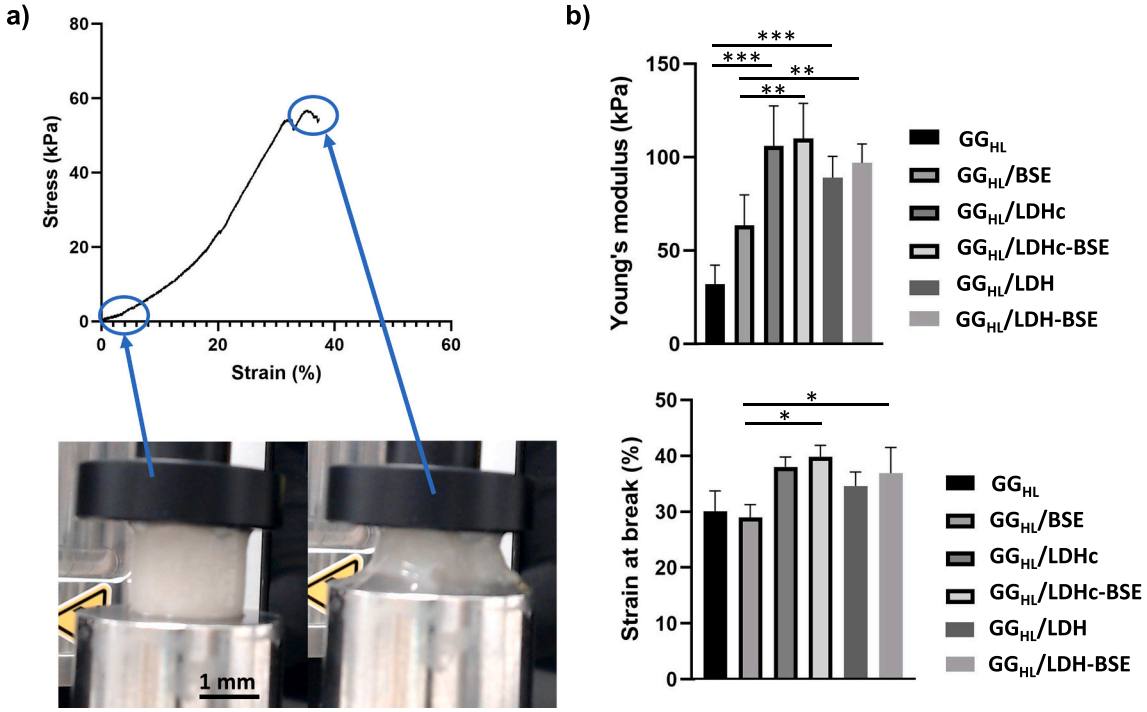

Fig. 6. On the top, stress-strain curve of the sample GG_{HL}/LDHc-BSE obtained by static compression test. On the bottom, pictures of the hydrogel at the start and at the end (just before reaching the break) of the compression test (a). Calculated values of the elastic compressive modulus and strain at break (b).

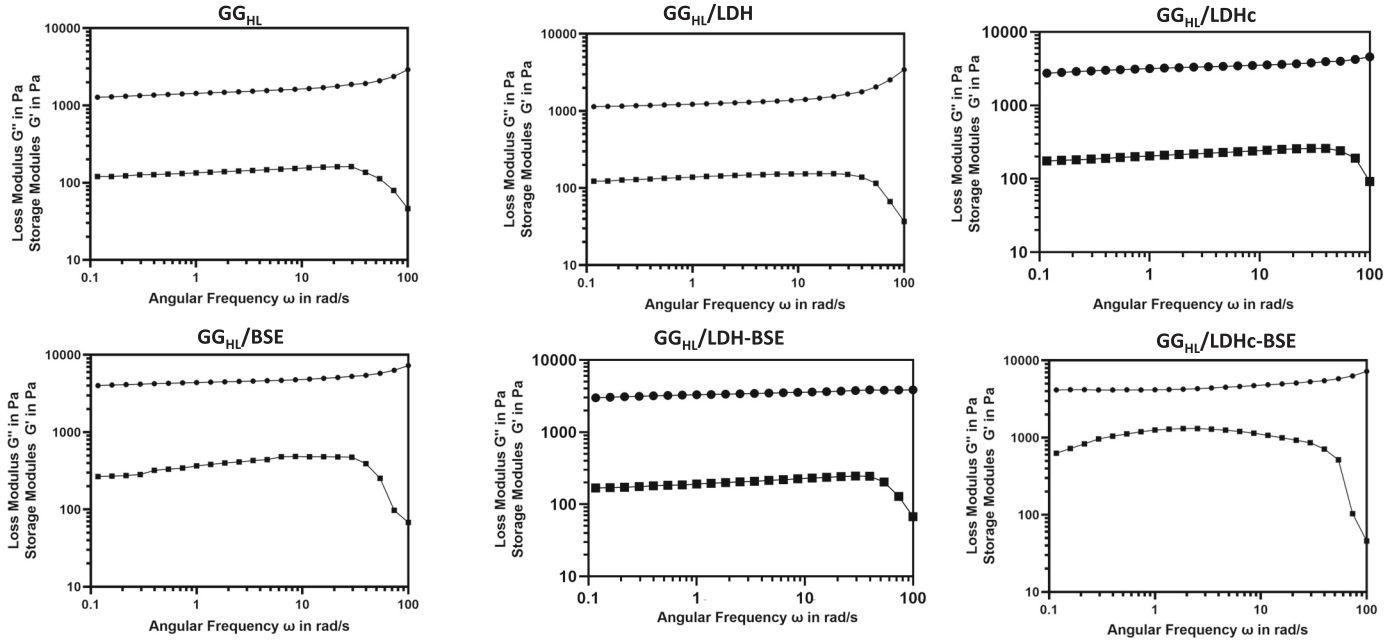

Fig. 7. Frequency sweep test using angular frequencies (ω) from 100 to 0.1 rad/s and a strain value within the linear viscoelastic region of 1 %.

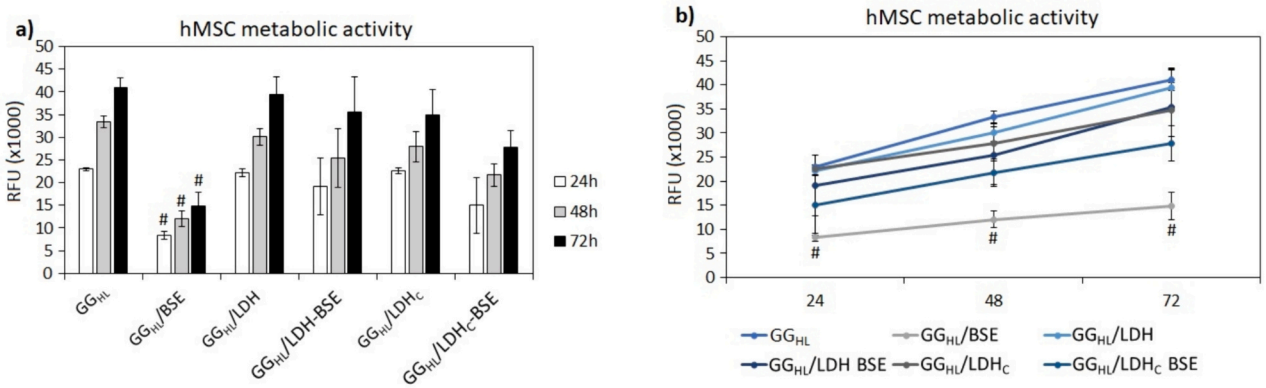

Fig. 8. Cytocompatibility. (a) The BSE loading did not cause toxic effects when the LDH systems (GG$_{HL}$/LDH-BSE and GG$_{HL}$/LDHc-BSE) were applied in comparison to the unloaded GG$_{HL}$ controls ($p > 0.05$); conversely, the free-BSE loaded composites (GG$_{HL}$/BSE) determined a significant reduction of the metabolic activity ($p < 0.05$, indicated by #). (b) However, results displayed in function of time showed that cells increased their metabolism within all the composites over time demonstrating a cells-friendly behavior. Bars represent means ± dev.st of 6 replicates.

and LDH-containing systems (Fig. 8a, $p < 0.05$ indicated by #) at each time-points. These results can suggest for a toxic effect of the GG$_{HL}$/BSE composites but looking at the data displayed in function of time (Fig. 8b), it can be observed that, for all the tested composites, an increase of the cells' metabolic activity was noticed over the subsequent time-points (24–48-72 h). So, all the composites seem to be cells-friendly and the observed reduction of the metabolic activity reported by the GG$_{HL}$/BSE specimens can related with the better control of BSE release that can be achieved by the LDH systems. In fact, previous literature reported that BSE can slow down cells' metabolic activity with an accentuated effect towards tumorigenic stem-like cells [46]; here, for biological assays we applied hTERT immortalized stem cells that are comparable to the ones cited by the above-mentioned literature, suggesting for a high sensibility to the BSE. So, considering the ability of the LDH systems to better control the release of the BSE over time, the reduction of metabolic activity can be due to the higher BSE amount release in a lower time from the GG$_{HL}$/BSE composites (as reported in Section 3.3).

To further demonstrate that composites represent suitable scaffolds hosting cells in a 3D environment, after 72 h cultivation the fluorescent live/dead assay was applied to visualize seeded cells within the pores by confocal microscopy. Results are summarized in Fig. 9.

In general, it was possible to observe viable cells (stained in green) at high density and homogeneously distributed within the entire areas of the pores where the images were collected (Fig. 9a–f, left column). The high density of cells successfully colonizing the scaffolds' pores was confirmed by the cells/area count performed using the ImageJ software as reported in the Supplementary Information (Fig. S5).

The 3D view of the cells' distribution further confirmed that hMSC were not growing as a monolayer but in a 3D conformation, following the topography provided by the materials architecture (Fig. 9a–f, right column). So, all the specimens were considered as cytocompatible and investigated for their anti-inflammatory and chondrogenic properties.

3.5.2. *Anti-inflammatory evaluation*

As previously discussed in the Introduction section, cartilage integrity can be highly hindered by inflammation due to oxidative stress; *in vivo* studies demonstrated that due to the pro-inflammatory

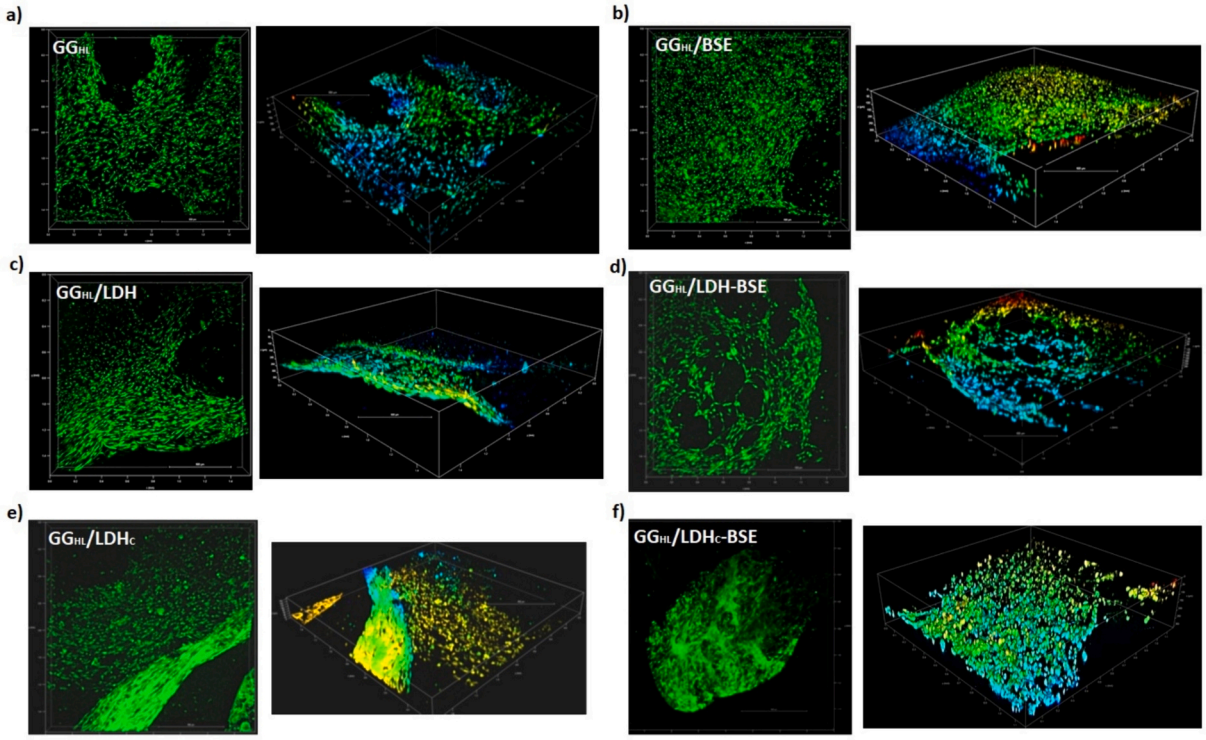

Fig. 9. Confocal microscopy. (a–f) After 72 h 3D cultivation within composites' pores cells were stained by the live/dead fluorescent assay. Images demonstrated that the majority of cells were viable (left columns, stained in green) as well as they homogeneously occupied the pores following the materials' topography as reported in the 3D arrangement (right columns, the different colors represent the cells different levels reconstructed by the *Z*-stack). Images bar scale = 500 μm.

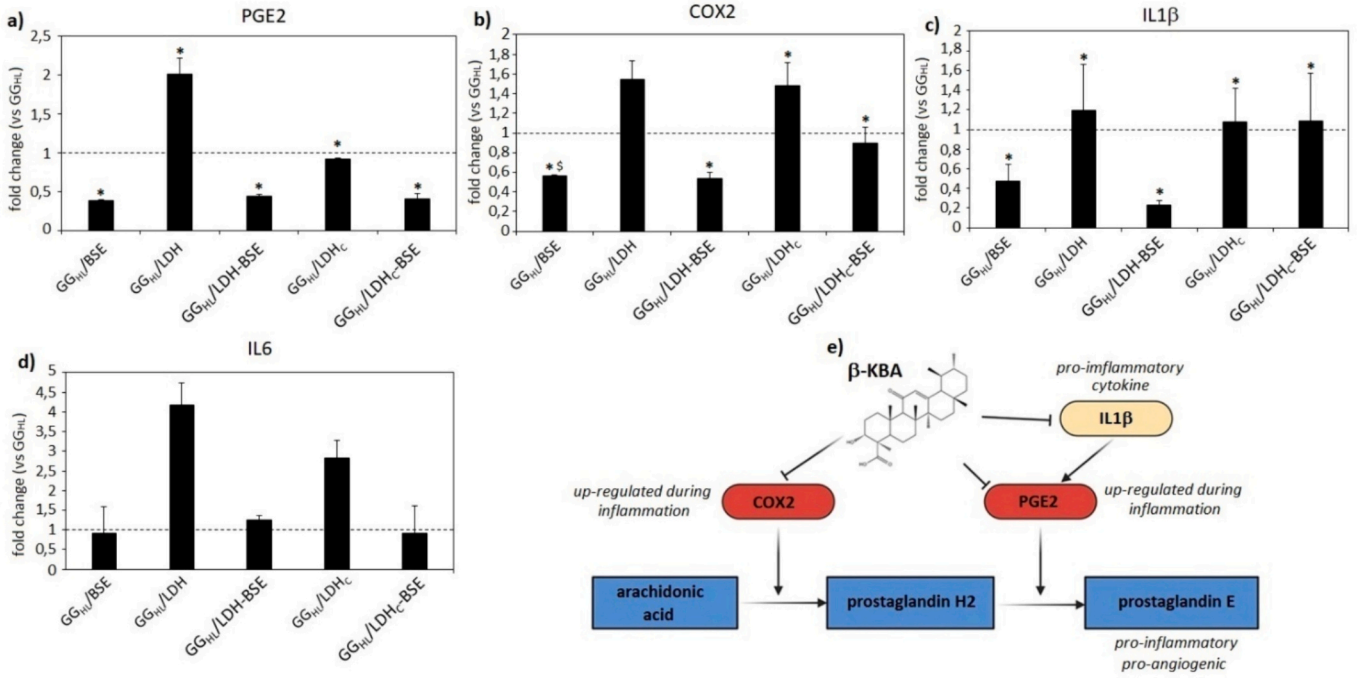

Fig. 10. BSE anti-inflammatory modulation. (a–d) The BSE-loaded composites (GG_{HL}/BSE, GG_{HL}/LDH-BSE and GG_{HL}/LDHc-BSE) reported a down-regulation of the tested pro-inflammatory genes, whereas on the opposite specimens lacking BSE displayed an up-regulation confirming the direct role of BSE in modulating gene expression. (e) Such results can be correlated with the well-known ability of BSE to suppress PGE2 thus impairing all the other related cascades such as COX2 and Il1β. Statistical analysis performed on quantification cycles (Cq): * = significant *vs* GGHL $p < 0.01$.

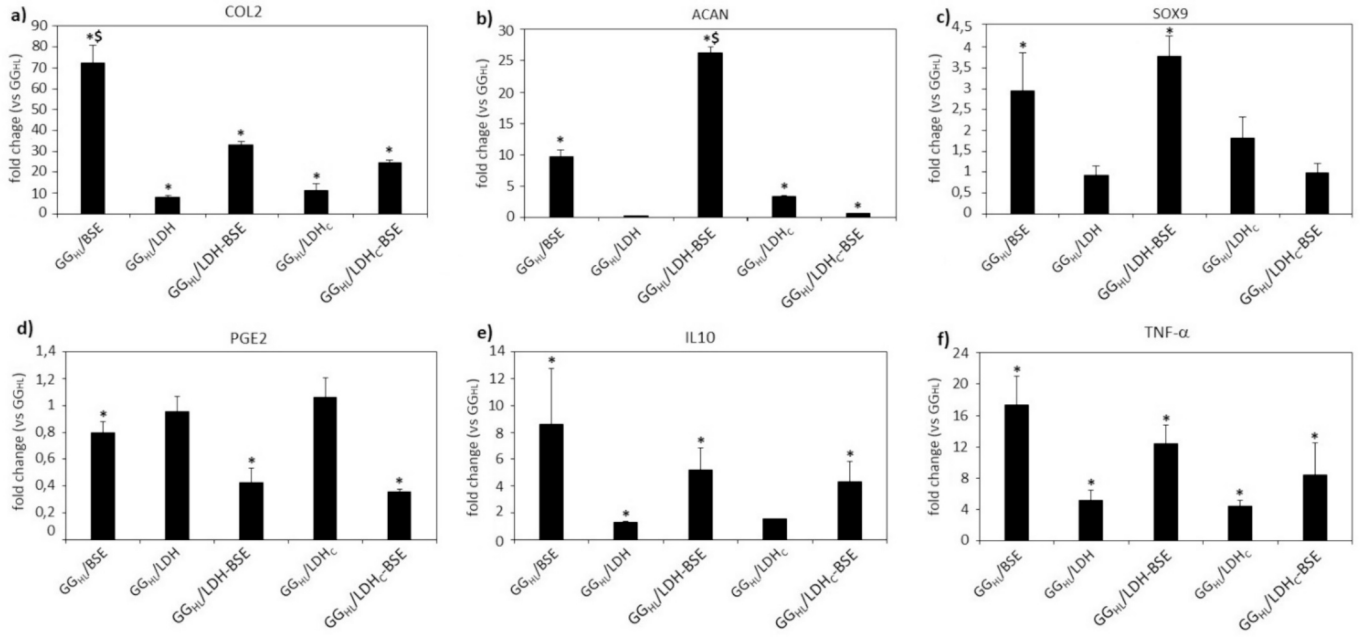

Fig. 11. Chondrogenesis. (a–c) The BSE-loaded GG_{HL}-BSE and GG_{HL}/LDH-BSE reported a strong up-regulation of all the tested chondrogenic genes in comparison to the unloaded GG_{HL} and GG_{HL}/LDH, thus suggesting for a pro-differentiation role of the BSE itself. Results are reported as fold change in comparison to the GG_{HL} control by the $2^{-\Delta\Delta CT}$ method. Pro/anti-inflammatory pathways modulation during chondrogenesis. (d–f) The BSE-loaded composites were able to modulate the differentiation route by down-regulating the pro-inflammatory PGE2 (d) and by up-regulating the anti-inflammatory IL10 (e). Conversely, the pro-inflammatory TNFa was up-regulated by the BSE (f), but it can be also boost chondrogenesis. Results are reported as fold change in comparison to the GGHL control by the $2^{-\Delta\Delta CT}$ method. Statistical analysis performed on quantification cycles (Cq): * = significant *vs* GG_{HL} $p < 0.01$; $ significant *vs* doped materials $p < 0.01$.

environment, cartilage injuries can fast worsen into chronic conditions leading to osteoarthritis [47]. Accordingly, materials aimed at cartilage repair should be able to modulate *in-situ* the expression of pro-inflammatory genes in order to prevent tissue degradation due to excessive recruitments of immune cells activated by the pro-inflammatory signals from the resident cells dealing with the implanted material [48]. BSE represents a well-known natural compound often administrated to counteract inflammation; so, oxidative stress was generated *via* ROS into the 3D models reported in Section 3.5.1 with the aim to evaluate the impact of the BSE in down-regulating the pro-inflammatory genes PGE2, COX2 and IL1β. Results are reported in Fig. 10. In general, the presence of BSE (GG_{HL}/BSE, GG_{HL}/LDH-BSE and GG_{HL}/LDHc-BSE) was successful in down-regulating (or at least in preventing the up-regulation) of pro-inflammatory genes in comparison to the unloaded GG_{HL}/LDH and GG_{HL}/LDHc (Fig. 10a–d). Results were normalized to the GG_{HL} control expression by the $2^{-\Delta\Delta ct}$ method, therefore fold change = 1 was considered as the threshold defining up- and down-regulation. Accordingly, the GG_{HL}/BSE and the GG_{HL}/LDH-BSE composites reported a general down-regulation of the PGE2, COX2 and IL1β genes; similarly, the GG_{HL}/LDHc-BSE composites displayed a down-regulation of PGE2 and COX2. Only IL6 was expressed in a comparable manner to the unloaded controls. On the opposite, the lack of BSE determined an up-regulation of all the tested genes, being their expression >1 threshold. These clearly contrary results provided a very promising preliminary evidence of the BSE direct involvement in the modulation of the inflammatory cascade by regulating the expression of pro-inflammatory genes.

These findings can be correlated with the ability of the BSE to directly inactivate the Prostaglandin E (PGE) as schematized in Fig. 10e. PGE is strongly related with inflammation and pain as well; its biosynthesis strictly depend by the activity of Cyclooxygenase 2 (COX2) and Prostaglandin E Synthase 2 (PGE2). In detail, arachidonic acid (AA) is released from the membrane phospholipids and converted *via* COX2 in prostaglandin H2 (PGH2); afterwards, it is further isomerized by PGE2 in PGE. Moreover, Interleukin I-beta (IL1β) can boost such pathway by up-regulating the expression of PGE2, thus increasing the production of PGE. In this scenario, Siemoneit et al. demonstrated that BSE could act as inhibitor of PGE2, thus suppressing all the related pathways leading to the release of the pro-inflammatory prostaglandin E [49]. Our results showed that the BSE loaded into the composites determined the down-regulation of both the mentioned genes COX2 and PGE2 indeed, thus confirming previous finding and providing a logical explanation to our findings.

Dealing with the interleukins-regulated pathways, Sharma et al. reported that BAs can partially inhibit in a dose-dependent manner (10 μM) the expression of IL6 [50], a pleiotropic cytokine produced in the initial stage of inflammation. Here, we did not obtain an indisputable down-regulation of IL6 and this can be due to the evidence that the β-KBA dose released from the composites does not reach the effectiveness target (see Fig. 5). However, we investigated the expression of IL1β showing a BSE-related down-regulation; considering that it represents a booster of the PGE2 activation, we can confirm that a further interference in the pro-inflammatory cascade can be due to the BSE *via* IL1β inhibition.

In conclusion, although a deeper *in vivo* validation is still necessary to confirm these results in a more complex systemic environment, by the reported data it can be speculated that BSE-loaded composites represent a promising strategy for the *in-situ* management of inflammation for cartilage tissue engineering.

3.5.3. *Chondrogenesis evaluation*

After demonstrating the composites' cytocompatibility and the efficacy of the loaded BSE to *in-situ* modulate the inflammatory cascade by down-regulating the COX2 and PGE2 gene expression, the ability of the scaffolds to support hMSC chondrogenesis was evaluated. The role of BSE was considered of particular interest because, at the best of our knowledge, only a very limited literature provided evidence of its role in promoting/supporting chondrogenesis. Kim et al. [51] showed that a combination of vitamin D, *Lactobacillus rhamnosus*, ginger, curcumin and Boswellia extract enhanced hMSC osteochondral differentiation;

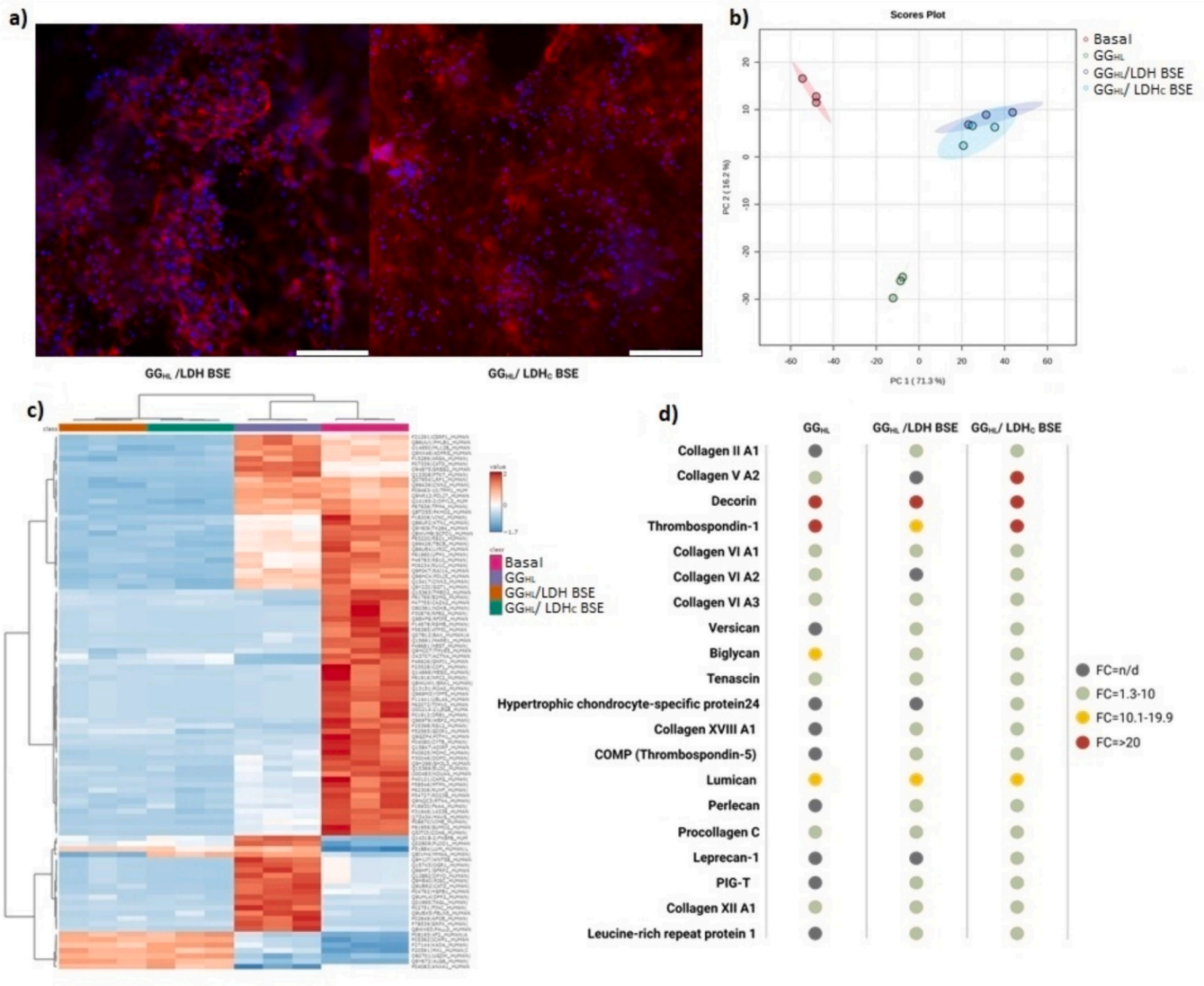

Fig. 12. Immunofluorescence (IF) and proteomics studies of chondrogenesis. (a) IF images of type 2 collagen synthesis and distribution in the BSE-doped scaffolds; (b) PCA analysis illustrating data distribution and homogeneity; (c) protein expression heatmap; (d) comparison of expression levels of cartilage-related proteins between basal and GGHL, GGHL/LDH BSE, and GGHL/LDHC BSE. FC = fold change. Images scale bar = 130 μm.

interestingly, the Authors suggested that such pro-regenerative boost was due to the cocktail strong anti-oxidative stress efficacy, thus showing a very promising confirmation of our findings. Similarly, Bi et al. [52] reported about the enhanced chondrogenic hMSC differentiation of cells in direct contact with BSE-loaded hydroxyapatite carboxymethyl cellulose composites, even if in this work the Authors did not correlated results with an anti-inflammatory effect due to the BSE release. In our work, we verified the expression of 3 of the main chondrogenic genes: collagen type II (COL2) representing the most abundant protein of the cartilage matrix, aggrecan (ACAN) that is the most common proteoglycan in the articular cartilage and SRY-Box Transcription Factor 9 (SOX9) that is known being a pivotal gene for chondrogenic differentiation over the osteogenic one. Results demonstrated that the BSE loading can be effectively related with an up-regulation of such genes as reported in Fig. 11a–c. Gene expression was normalized towards the unloaded GG_{HL} control; therefore, it can be speculated that the observed up-regulations are mostly due to the modifications introduced to the composites. Accordingly, the BSE-loaded composites GG_{HL}/BSE and GG_{HL}/LDH-BSE reported an up-regulation of all the tested genes in comparison to the same composites without BSE (GG_{HL} and GG_{HL}/LDH), thus clearly suggesting for a boost effect due to the BSE. Regarding the GG_{HL}/LDHc-BSE composites, they reported an up-regulation of the COL2 in comparison to the unloaded composites (GG_{HL}/LDHc), but a similar expression for ACAN and SOX9, thus being less effective in promoting hMSC differentiation.

To support the results obtained from real-time PCR, the presence of cartilage-like collagen type 2 in BSE-doped scaffolds was firstly verified using immunofluorescence. The results demonstrated robust synthesis and distribution of type 2 collagen along the scaffold network as shown in Fig. 12a representing the 3D reconstruction from the confocal microscope; in particular, GG_{HL}/LDH BSE specimens suggest a higher expression of collagen as can be appreciated in the movie reported in the Supplementary file SM1.

However, PCR results suggested for both pro-regenerative and anti-inflammatory regulated pathways due to the *Boswellia* activity, therefore proteomics studies were exploited to the scaffolds imposed to chondrogenic differentiation to verify if such genetic studies were confirmed at the level of expressed proteins. Accordingly, results from the Principal Component Analysis (PCA) illustrated in Fig. 12b reveals a highly diverse proteomic profile among the scaffolds, with the datasets of GG_{HL}/LDH BSE and GG_{HL}/LDH_C BSE exhibiting significant overlap. This difference highlighted by the PCA is further demonstrated by the

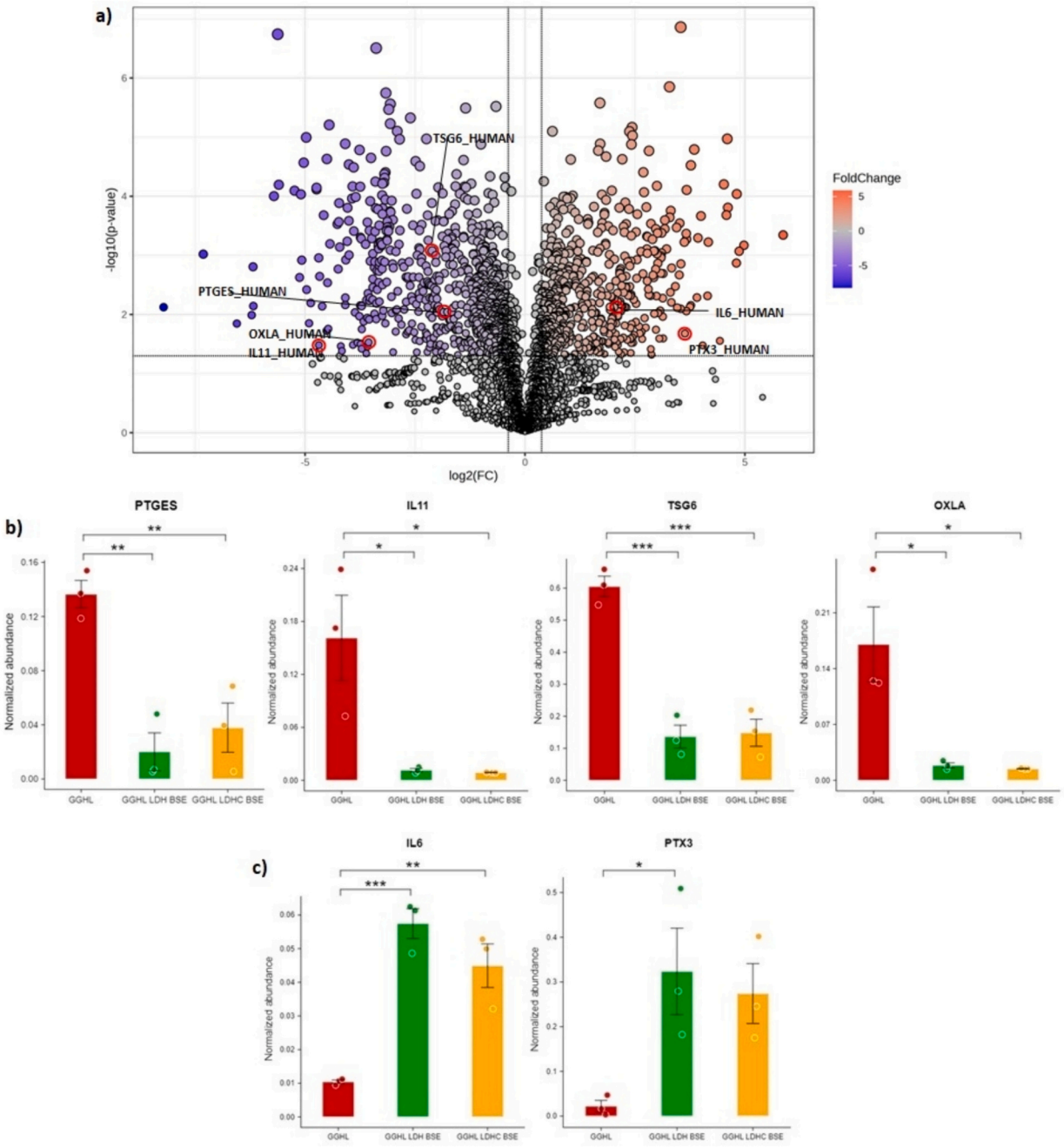

Fig. 13. Proteomic analysis for immunomodulation. (a) Volcano plot displaying differentially expressed proteins in the comparison between GG_{HL} and GG_{HL}/LDH BSE. (b–c) Pro- and anti-inflammatory proteins significantly up- or down-regulated between specimens. *$p < 0.05$; ** $p < 0.01$; ***p 0.001.

heatmap reported in Fig. 12c. It is reasonable to hypothesize that the difference observed is strictly correlated with the presence of BSE in the scaffolds. The dot plot illustrated in Fig. 12c shows the comparison of expression levels (reported as fold changes) of detected cartilage-related proteins when Basal is compared to GG_{HL}, GG_{HL}/LDH BSE, or GG_{HL}/LDH_C BSE. The results demonstrate that both BSE-doped scaffolds express significantly higher levels proteins highly relevant for cartilage such as Collagen II, Cartilage Oligomeric Matrix Protein (COMP), Perlecan, Versican, and Leucine-rich repeat protein 1. Very interesting, the up-regulation of such cartilage related proteins is less marked when GG_{HL} specimens are compared to the Basal control; on the opposite, the up-regulation is more evident by comparing BSE-doped specimens to the Basal control, thus suggesting for a direct effect of the BSE in improving the differentiation route.

Based on these findings, to understand how BSE can modulate the differentiation route, we came back to the loaded composites anti-inflammatory properties previously shown in Fig. 10. In fact, although chondrogenesis was not carried out under oxidative stress conditions like previous tests, it is known that despite TGFβ in necessary for the chondrogenic medium to promote differentiation and protect from senescence, it may induce inflammation in combination with interleukins (such as IL6 and IL1) as reported by a large literature [53–55]. So, we hypothesized that the beneficial effect provided by the BSE for the chondrogenic differentiation could be related to its ability to modulate such inflammation. Accordingly, the expression of the pro-inflammatory genes Prostaglandin E Synthase 2 (PGE2) and Tumor Necrosis Factor alpha (TNFα) were evaluated as well as the regulation of the anti-inflammatory Interleukin 10 (IL10) was detected, too. Results

are reported in Fig. 11d–f.

Interestingly, when the BSE-loaded composites were considered, the regulation of PGE2 (Fig. 11d) and IL10 (Fig. 11e) was essentially the opposite; in fact, the pro-inflammatory PGE2 was down-regulated (fold change <1), whereas the anti-inflammatory IL10 was up-regulated. So, we can hypothesize that the BSE loading can effectively modulate the inflammation by affecting the genetic expression of genes involved both in the activation (PGE2) and de-activation (IL10) of the cascade. Finally, the results related to the TNFα expression are less clear and more difficult to interpret. Indeed, the BSE loading determined an up-regulation of this pro-inflammatory gene, thus suggesting a contradiction to what was discussed previously. However, some literature such as Jagielski et al. [56] demonstrated that hMSC chondrogenic differentiation can be boosted by alternative pathways such as IL10 and TNFα that was not reported inducing inflammation.

Afterwards, as previously reported for chondrogenic studies, proteomics was exploited to correlate the observed regulation of anti- and pro-inflammatory genes and the expressed proteins. Accordingly, the volcano plot (Fig. 13a) includes up- and down-regulated pro- and anti-inflammatory proteins identified in the comparison between GG_{HL} and GG_{HL}/LDH BSE and GG_{HL}/LDH_C BSE. Results demonstrate that both BSE-doped scaffolds exhibit an up-regulation of Prostaglandin-E Synthase (PTGES), IL11, Tumor necrosis factor-stimulated gene 6 (TSG6), and Interleukin-4-induced protein 1 (OXLA), which are known to be up-regulated in inflammatory conditions [57,58] as reported in Fig. 13b. Moreover, BSE-doped scaffolds induced an up-regulation of Pentraxin 3 (PTX3), an acute-phase protein expressed in response to pro-inflammatory stimuli [59], and IL6, a multifunctional protein with both anti-inflammatory and pro-inflammatory roles as reported in Fig. 13c. Notably, Kondo et al. [60] previously reported that IL6 overexpression may actively contribute to the chondrogenic differentiation of human mesenchymal stem cells, thus providing another interesting hint to the here observed pro-chondrogenic boost due to BSE loading.

So, taken into account all the presented results, it can be speculated that the BSE-loaded composites, with a particular reference to the GG_{HL}/LDH-BSE ones, can be considered as promising materials for cartilage tissue engineering being able to modulate the inflammatory reaction by the COX2 and PGE2 pathways. However, some unclear aspects, such as the correlation BSE-TNFα still remain; therefore, in the future, further studies will have to be specifically addressed to extend the comprehension of the expression of other inflammatory regulatory genes as well as the studies must be completed by the evaluation of immune cells reaction towards the materials *per se* and after the modulation of the released pro-inflammatory signals by *in vivo* models.

4. Conclusions

In this paper, GG-based composite hydrogels containing BSE, both in their free form and conveyed by LDH (as-such or calcined) clays, have been successfully investigated for their potential in cartilage tissue regeneration. The composites were characterized in terms of their structural, thermal, morphological, mechanical and biological properties. *In vitro* release studies evidenced a substantially similar controlled β-KBA release profile from GG_{HL}/LDH-BSE and GG_{HL}/LDHc-BSE into the SSFE medium. Moreover, both the unmodified and calcined LDH systems showed comparable enhancement of the mechanical properties compared with those without clays. Although the BSE presence did not change the composite's behavior under compressive tests, rheological results evidenced that the addition of the extract supplied more cohesive intermolecular polysaccharide interactions. Evaluation of the hydrogels' biological features, performed using hMSC cells, showed that the presence of BSE provided good cytocompatibility when loaded in LDH or LDHc systems. Anti-inflammatory studies pointed out that BSE was successful in down-regulating pro-inflammatory genes. Finally, chondrogenesis studies demonstrated an enhanced differentiation, especially in the case of GG_{HL}/LDH-BSE, leading to the up-regulation of COL 2 and ACAN. Proteomics confirmed the pro-regenerative and anti-inflammatory signature of the proteins expressed by the cells cultivated into the BSE-loaded specimens. These preliminary *in vitro* investigations demonstrated that GG_{HL}/LDH-BSE could represent a promising BSE delivery system exhibiting an interesting combination of mechanical and biological properties for cartilage repair applications.

Supplementary data to this article can be found online at https://doi.org/10.1016/j.ijbiomac.2024.134079.

CRediT authorship contribution statement

Stefania Cometa: Conceptualization, Data curation, Investigation, Methodology, Writing – original draft, Writing – review & editing. **Francesco Busto:** Data curation, Investigation, Methodology, Writing – original draft. **Alessandro C. Scalia:** Data curation, Investigation, Methodology, Writing – original draft. **Andrea Castellaneta:** Data curation, Investigation, Methodology, Writing – original draft. **Piergiorgio Gentile:** Data curation, Funding acquisition, Investigation, Methodology, Writing – original draft, Writing – review & editing. **Andrea Cochis:** Data curation, Investigation, Methodology, Writing – original draft, Writing – review & editing. **Marcello Manfredi:** Data curation, Investigation, Writing – original draft. **Vittoria Borrini:** Data curation, Investigation, Writing – original draft. **Lia Rimondini:** Funding acquisition, Writing – original draft. **Elvira De Giglio:** Conceptualization, Funding acquisition, Supervision, Writing – original draft, Writing – review & editing.

Declaration of competing interest

The authors declare that they have no known competing financial interests or personal relationships that could have appeared to influence the work reported in this paper.

Data availability

Data will be made available on request.

References

[1] H. Utsunomiya, K.K. Briggs, G.J. Dornan, I.K. Bolia, R. Locks, M.J. Philippon, Predicting severe cartilage damage in the hip: a model using patient-specific data from 2,396 hip arthroscopies, Arthroscopy: The Journal of Arthroscopic & Related Surgery 35 (2019) 2051–2060.e13, https://doi.org/10.1016/j.arthro.2019.02.033.
[2] Y.A. Pei, S. Chen, M. Pei, The essential anti-angiogenic strategies in cartilage engineering and osteoarthritic cartilage repair, Cell. Mol. Life Sci. 79 (2022) 71, https://doi.org/10.1007/s00018-021-04105-0.
[3] J. Samuels, M.H. Pillinger, D. Jevsevar, D. Felson, L.S. Simon, Critical appraisal of intra-articular glucocorticoid injections for symptomatic osteoarthritis of the knee, Osteoarthr. Cartil. 29 (2021) 8–16, https://doi.org/10.1016/j.joca.2020.09.001.
[4] D.A. Prince, I.J. Villamagna, A. Borecki, F. Beier, J.R. De Bruyn, M. Hurtig, E. R. Gillies, Thermoresponsive and covalently cross-linkable hydrogels for intra-articular drug delivery, ACS Appl. Bio Mater. 2 (2019) 3498–3507, https://doi.org/10.1021/acsabm.9b00410.
[5] M. Majeed, S. Majeed, N.K. Narayanan, K. Nagabhushanam, A pilot, randomized, double-blind, placebo-controlled trial to assess the safety and efficacy of a novel *Boswellia serrata* extract in the management of osteoarthritis of the knee, Phytother. Res. 33 (2019) 1457–1468, https://doi.org/10.1002/ptr.6338.
[6] G. Yu, W. Xiang, T. Zhang, L. Zeng, K. Yang, J. Li, Effectiveness of Boswellia and Boswellia extract for osteoarthritis patients: a systematic review and meta-analysis, BMC Complement Med Ther 20 (2020) 225, https://doi.org/10.1186/s12906-020-02985-6.
[7] Y. Henrotin, A. Mobasheri, Natural products for promoting joint health and managing osteoarthritis, Curr. Rheumatol. Rep. 20 (2018) 72, https://doi.org/10.1007/s11926-018-0782-9.
[8] D. Poeckel, O. Werz, Boswellic acids: biological actions and molecular targets, CMC 13 (2006) 3359–3369, https://doi.org/10.2174/092986706779010333.
[9] N. Kimmatkar, V. Thawani, L. Hingorani, R. Khiyani, Efficacy and tolerability of Boswellia serrata extract in treatment of osteoarthritis of knee – a randomized double blind placebo controlled trial, Phytomedicine 10 (2003) 3–7, https://doi.org/10.1078/094471103321648593.
[10] D. Trucco, L. Riacci, L. Vannozzi, C. Manfredi, L. Arrico, E. Gabusi, G. Lisignoli, L. Ricotti, Primers for the adhesion of gellan gum-based hydrogels to the cartilage: a comparative study, Macromol. Biosci. 22 (2022) 1616–5187, https://doi.org/10.1002/mabi.202200096.

[11] M.A. Bonifacio, P. Gentile, A.M. Ferreira, S. Cometa, E. De Giglio, Insight into halloysite nanotubes-loaded gellan gum hydrogels for soft tissue engineering applications, Carbohydr. Polym. 163 (2017) 280–291, https://doi.org/10.1016/j.carbpol.2017.01.064.
[12] M.A. Bonifacio, S. Cometa, A. Cochis, P. Gentile, A.M. Ferreira, B. Azzimonti, G. Procino, E. Ceci, L. Rimondini, E. De Giglio, Antibacterial effectiveness meets improved mechanical properties: Manuka honey/gellan gum composite hydrogels for cartilage repair, Carbohydr. Polym. 198 (2018) 462–472, https://doi.org/10.1016/j.carbpol.2018.06.115.
[13] M.A. Bonifacio, A. Cochis, S. Cometa, A. Scalzone, P. Gentile, G. Procino, S. Milano, A.C. Scalia, L. Rimondini, E. De Giglio, Advances in cartilage repair: the influence of inorganic clays to improve mechanical and healing properties of antibacterial Gellan gum-Manuka honey hydrogels, Mater. Sci. Eng. C 108 (2020) 110444, https://doi.org/10.1016/j.msec.2019.110444.
[14] M.A. Bonifacio, A. Cochis, S. Cometa, P. Gentile, A. Scalzone, A.C. Scalia, L. Rimondini, E. De Giglio, From the sea to the bee: gellan gum-honey-diatom composite to deliver resveratrol for cartilage regeneration under oxidative stress conditions, Carbohydr. Polym. 245 (2020) 116410, https://doi.org/10.1016/j.carbpol.2020.116410.
[15] M.A. Bonifacio, S. Cometa, A. Cochis, A. Scalzone, P. Gentile, A.C. Scalia, L. Rimondini, P. Mastrorilli, E. De Giglio, A bioprintable gellan gum/lignin hydrogel: a smart and sustainable route for cartilage regeneration, Int. J. Biol. Macromol. 216 (2022) 336–346, https://doi.org/10.1016/j.ijbiomac.2022.07.002.
[16] R.K. Kankala, Nanoarchitectured two-dimensional layered double hydroxides-based nanocomposites for biomedical applications, Adv. Drug Deliv. Rev. 186 (2022) 114270, https://doi.org/10.1016/j.addr.2022.114270.
[17] T. Zhao, S. Zhang, Y. Guo, Q. Wang, TiC_2 : a new two-dimensional sheet beyond MXenes, Nanoscale 8 (2016) 233–242, https://doi.org/10.1039/C5NR04472C.
[18] P. Liu, M. Li, H. Yu, H. Fang, J. Yin, D. Zhu, Q. Yang, Q. Ke, Y. Huang, Y. Guo, Y. Gao, C. Zhang, Biphasic CK2.1-coated β-glycerophosphate chitosan/LL37-modified layered double hydroxide chitosan composite scaffolds enhance coordinated hyaline cartilage and subchondral bone regeneration, Chem. Eng. J. 418 (2021) 129531, https://doi.org/10.1016/j.cej.2021.129531.
[19] S.S. Lee, G.E. Choi, H.J. Lee, Y. Kim, J.-H. Choy, B. Jeong, Layered double hydroxide and polypeptide thermogel nanocomposite system for chondrogenic differentiation of stem cells, ACS Appl. Mater. Interfaces 9 (2017) 42668–42675, https://doi.org/10.1021/acsami.7b17173.
[20] S. Cometa, F. Busto, A. Castellaneta, A. Cochis, Z. Najmi, R. Rizzi, I. Losito, E. De Giglio, Development, analytical characterization, and bioactivity evaluation of Boswellia serrata extract-layered double hydroxide hybrid composites, Molecules 28 (2023) 6449, https://doi.org/10.3390/molecules28186449.
[21] M.R.C. Marques, R. Loebenberg, M. Almukainzi, Simulated biological fluids with possible application in dissolution testing, Dissolution Technol. 18 (2011) 15–28, https://doi.org/10.14227/DT180311P15.
[22] A. Asteggiano, L. Curatolo, V. Schiavo, A. Occhipinti, C. Medana, Development, validation, and application of a simple and rugged HPLC method for boswellic acids for a comparative study of their abundance in different species of Boswellia gum resins, Appl. Sci. 13 (2023) 1254, https://doi.org/10.3390/app13031254.
[23] S. James, J. Fox, F. Afsari, J. Lee, S. Clough, C. Knight, J. Ashmore, P. Ashton, O. Preham, M. Hoogduijn, R.D.A.R. Ponzoni, Y. Hancock, M. Coles, P. Genever, Multiparameter analysis of human bone marrow stromal cells identifies distinct immunomodulatory and differentiation-competent subtypes, Stem Cell Rep. 4 (2015) 1004–1015, https://doi.org/10.1016/j.stemcr.2015.05.005.
[24] S.S. Narasagoudr, V.G. Hegde, V.N. Vanjeri, R.B. Chougale, S.P. Masti, Influence of Boswellic acid on physical, structural and morphological properties of poly (vinyl alcohol) films, Chemical Data Collections 27 (2020) 100370, https://doi.org/10.1016/j.cdc.2020.100370.
[25] A. Tambe, N. Pandita, P. Kharkar, N. Sahu, Encapsulation of boswellic acid with β- and hydroxypropyl-β-cyclodextrin: synthesis, characterization, in vitro drug release and molecular modelling studies, J. Mol. Struct. 1154 (2018) 504–510, https://doi.org/10.1016/j.molstruc.2017.10.061.
[26] M. Avella, E.D. Pace, B. Immirzi, G. Impallomeni, M. Malinconico, G. Santagata, Addition of glycerol plasticizer to seaweeds derived alginates: influence of microstructure on chemical–physical properties, Carbohydr. Polym. 69 (2007) 503–511, https://doi.org/10.1016/j.carbpol.2007.01.011.
[27] R. Russo, A. Giuliani, B. Immirzi, M. Malinconico, G. Romano, Alginate/polyvinylalcohol blends for agricultural applications: structure-properties correlation, mechanical properties and greenhouse effect evaluation, Macromol. Symp. 218 (2004) 241–250, https://doi.org/10.1002/masy.200451425.
[28] B.A. Shah, G.N. Qazi, S.C. Taneja, Boswellic acids: a group of medicinally important compounds, Nat. Prod. Rep. 26 (2009) 72–89, https://doi.org/10.1039/B809437N.
[29] M. Schmiech, J. Ulrich, S.J. Lang, B. Büchele, C. Paetz, A. St-Gelais, T. Syrovets, T. Simmet, 11-Keto-α-boswellic acid, a novel triterpenoid from Boswellia spp. with chemotaxonomic potential and antitumor activity against triple-negative breast cancer cells, Molecules 26 (2021) 366, https://doi.org/10.3390/molecules26020366.
[30] Y. Zhang, Z. Ning, C. Lu, S. Zhao, J. Wang, B. Liu, X. Xu, Y. Liu, Triterpenoid resinous metabolites from the genus Boswellia: pharmacological activities and potential species-identifying properties, Chem. Cent. J. 7 (2013) 153, https://doi.org/10.1186/1752-153X-7-153.
[31] C. Zhang, L. Sun, R. Tian, H. Jin, S. Ma, B. Gu, Combination of quantitative analysis and chemometric analysis for the quality evaluation of three different frankincenses by ultra high performance liquid chromatography and quadrupole time of flight mass spectrometry: liquid chromatography, J. Sep. Sci. 38 (2015) 3324–3330, https://doi.org/10.1002/jssc.201500326.
[32] F. Börner, M. Werner, J. Ertelt, J. Meins, M. Abdel-Tawab, O. Werz, Analysis of boswellic acid contents and related pharmacological activities of frankincense-based remedies that modulate inflammation, Pharmaceuticals 14 (2021) 660, https://doi.org/10.3390/ph14070660.
[33] M. Schmiech, S.J. Lang, K. Werner, L.J. Rashan, T. Syrovets, T. Simmet, Comparative analysis of pentacyclic triterpenic acid compositions in oleogum resins of different Boswellia species and their in vitro cytotoxicity against treatment-resistant human breast cancer cells, Molecules 24 (2019) 2153, https://doi.org/10.3390/molecules24112153.
[34] H.P.T. Ammon, Modulation of the immune system by Boswellia serrata extracts and boswellic acids, Phytomedicine 17 (2010) 862–867, https://doi.org/10.1016/j.phymed.2010.03.003.
[35] S. Schweizer, A.F.W. Von Brocke, S.E. Boden, E. Bayer, H.P.T. Ammon, H. Safayhi, Workup-dependent formation of 5-lipoxygenase inhibitory boswellic acid analogues, J. Nat. Prod. 63 (2000) 1058–1061, https://doi.org/10.1021/np000069k.
[36] T. Sharma, S. Jana, Investigation of molecular properties that influence the permeability and oral bioavailability of major β-boswellic acids, Eur. J. Drug Metab. Pharmacokinet. 45 (2020) 243–255, https://doi.org/10.1007/s13318-019-00599-z.
[37] T. Coradin, K. Wang, T. Law, L. Trichet, Type I collagen-fibrin mixed hydrogels: preparation, properties and biomedical applications, Gels 6 (2020) 36, https://doi.org/10.3390/gels6040036.
[38] A. Scalzone, A.M. Ferreira, C. Tonda-Turo, G. Ciardelli, K. Dalgarno, P. Gentile, The interplay between chondrocyte spheroids and mesenchymal stem cells boosts cartilage regeneration within a 3D natural-based hydrogel, Sci. Rep. 9 (2019) 14630, https://doi.org/10.1038/s41598-019-51070-7.
[39] T.-A.N. Kelly, B.L. Roach, Z.D. Weidner, C.R. Mackenzie-Smith, G.D. O'Connell, E. G. Lima, A.M. Stoker, J.L. Cook, G.A. Ateshian, C.T. Hung, Tissue-engineered articular cartilage exhibits tension–compression nonlinearity reminiscent of the native cartilage, J. Biomech. 46 (2013) 1784–1791, https://doi.org/10.1016/j.jbiomech.2013.05.017.
[40] C. Zhu, H. Lei, D. Fan, Z. Duan, X. Li, Y. Li, J. Cao, S. Wang, Y. Yu, Novel enzymatic crosslinked hydrogels that mimic extracellular matrix for skin wound healing, J. Mater. Sci. 53 (2018) 5909–5928, https://doi.org/10.1007/s10853-017-1956-y.
[41] G. Botta, B.M. Bizzarri, A. Garozzo, R. Timpanaro, B. Bisignano, D. Amatore, A. T. Palamara, L. Nencioni, R. Saladino, Carbon nanotubes supported tyrosinase in the synthesis of lipophilic hydroxytyrosol and dihydrocaffeoyl catechols with antiviral activity against DNA and RNA viruses, Bioorg. Med. Chem. 23 (2015) 5345–5351, https://doi.org/10.1016/j.bmc.2015.07.061.
[42] S. Fuchs, K. Shariati, M. Ma, Specialty tough hydrogels and their biomedical applications, Adv Healthcare Materials 9 (2020) 1901396, https://doi.org/10.1002/adhm.201901396.
[43] G. Stojkov, Z. Niyazov, F. Picchioni, R.K. Bose, Relationship between structure and rheology of hydrogels for various applications, Gels 7 (2021) 255, https://doi.org/10.3390/gels7040255.
[44] D. Pasqui, M. De Cagna, R. Barbucci, Polysaccharide-based hydrogels: the key role of water in affecting mechanical properties, Polymers 4 (2012) 1517–1534, https://doi.org/10.3390/polym4031517.
[45] J. Yu, X. Wang, D. Li, L. Wang, Y. Wang, Development of soy protein isolate emulsion gels as extrusion-based 3D food printing inks: effect of polysaccharides incorporation, Food Hydrocoll. 131 (2022) 107824, https://doi.org/10.1016/j.foodhyd.2022.107824.
[46] H. Schneider, M. Weller, Boswellic acid activity against glioblastoma stem-like cells, Oncol. Lett. 11 (2016) 4187–4192, https://doi.org/10.3892/ol.2016.4516.
[47] Oxidative stress in secondary osteoarthritis: from cartilage destruction to clinical presentation? Orthop. Rev. 2 (2010) https://doi.org/10.4081/or.2010.e23.
[48] R. Whitaker, B. Hernaez-Estrada, R.M. Hernandez, E. Santos-Vizcaino, K.L. Spiller, Immunomodulatory biomaterials for tissue repair, Chem. Rev. 121 (2021) 11305–11335, https://doi.org/10.1021/acs.chemrev.0c00895.
[49] U. Siemoneit, A. Koeberle, A. Rossi, F. Dehm, M. Verhoff, S. Reckel, T. Maier, J. Jauch, H. Northoff, F. Bernhard, V. Doetsch, L. Sautebin, O. Werz, Inhibition of microsomal prostaglandin E $_2$ synthase-1 as a molecular basis for the anti-inflammatory actions of boswellic acids from frankincense, British, Aust. J. Pharm. 162 (2011) 147–162, https://doi.org/10.1111/j.1476-5381.2010.01020.x.
[50] S. Sharma, S. Gupta, V. Khajuria, A. Bhagat, Z. Ahmed, B.A. Shah, Analogues of boswellic acids as inhibitors of pro-inflammatory cytokines TNF-α and IL-6, Bioorg. Med. Chem. Lett. 26 (2016) 695–698, https://doi.org/10.1016/j.bmcl.2015.11.035.
[51] D.H. Kim, D.H. Kim, B.E. Heck, M. Shaffer, J. Hur, K.H. Yoo, A natural supplement formula reduces anti-oxidative stress and enhances osteo-chondrogenic differentiation potential in mesenchymal stem cells, J. Clin. Biochem. Nutr. 66 (n. d.) 206–212. doi:https://doi.org/10.3164/jcbn.19-97.
[52] D. Bi, G. Chen, J. Cheng, J. Wen, N. Pei, H. Zeng, Y. Li, Boswellic acid captivated hydroxyapatite carboxymethyl cellulose composites for the enhancement of chondrocytes in cartilage repair, Arab. J. Chem. 13 (2020) 5605–5613, https://doi.org/10.1016/j.arabjc.2020.03.030.
[53] N. Thielen, P. Van Der Kraan, A. Van Caam, TGFβ/BMP signaling pathway in cartilage homeostasis, Cells 8 (2019) 969, https://doi.org/10.3390/cells8090969.
[54] S. Ashraf, B.-H. Cha, J.-S. Kim, J. Ahn, I. Han, H. Park, S.-H. Lee, Regulation of senescence associated signaling mechanisms in chondrocytes for cartilage tissue regeneration, Osteoarthr. Cartil. 24 (2016) 196–205, https://doi.org/10.1016/j.joca.2015.07.008.
[55] S. Liu, Z. Deng, K. Chen, S. Jian, F. Zhou, Y. Yang, Z. Fu, H. Xie, J. Xiong, W. Zhu, Cartilage tissue engineering: from proinflammatory and anti-inflammatory

cytokines to osteoarthritis treatments (review), Mol. Med. Rep. 25 (2022) 99, https://doi.org/10.3892/mmr.2022.12615.
[56] M. Jagielski, J. Wolf, U. Marzahn, A. Völker, M. Lemke, C. Meier, W. Ertel, O. Godkin, S. Arens, G. Schulze-Tanzil, The influence of IL-10 and TNFα on chondrogenesis of human mesenchymal stromal cells in three-dimensional cultures, IJMS 15 (2014) 15821–15844, https://doi.org/10.3390/ijms150915821.
[57] A.J. Day, C.M. Milner, TSG-6: a multifunctional protein with anti-inflammatory and tissue-protective properties, Matrix Biol. 78–79 (2019) 60–83, https://doi.org/10.1016/j.matbio.2018.01.011.
[58] A.F. Abdel-Magid, Inhibitors of interleukin 4 induced protein 1 (IL4I1) as potential treatment for cancer, ACS Med. Chem. Lett. 14 (2023) 127–128, https://doi.org/10.1021/acsmedchemlett.2c00525.
[59] A.L. Slusher, A.B. Mischo, E.O. Acevedo, Pentraxin 3 is an anti-inflammatory protein associated with lipid-induced interleukin 10 in vitro, Cytokine 86 (2016) 36–40, https://doi.org/10.1016/j.cyto.2016.07.012.
[60] M. Kondo, K. Yamaoka, K. Sakata, K. Sonomoto, L. Lin, K. Nakano, Y. Tanaka, Contribution of the interleukin-6/STAT-3 signaling pathway to chondrogenic differentiation of human mesenchymal stem cells, Arthritis, Rheumatol 67 (2015) 1250–1260, https://doi.org/10.1002/art.39036.